INVESTIGATING THE EFFECT OF DIFFERENT RHEOLOGICAL MODELS ON THE BLOOD FLOW IN CAPILLARY SEGMENTS

FARKLI REOLOJIK MODELLERIN KILCAL SEGMENTLERDEKI KAN AKIŞI ÜZERINDEKI ETKISININ INCELENMESI

Masah Omar Mustafa Abubaker

Assoc. Prof. Dr. Özgür Ekici

Supervisor

Assoc. Prof. Dr. Şefik Evren Erdener

Co-Supervisor

Submitted to

Graduate School of Science and Engineering of Hacettepe University

as a Partial Fulfilment to the Requirement

for the Award of the Degree of Master of Science

in Mechanical Engineering

2021

ÖZET

FARKLI REOLOJİK MODELLERİN KILCAL SEGMENTLERDEKİ KAN AKIŞI ÜZERİNDEKİ ETKİSİNİN İNCELENMESİ

Masah Omar Mustafa ABUBAKER

Yüksek Lisans, Makine Mühendisliği Bölümü

Tez Danışmanı: Assoc. Prof. Dr. Özgür Ekici

Eş Danışman: Assoc. Prof. Dr. Şefik Evren Erdener

Aralık 2021, 89 sayfa

Bu çalışma, kılcal damarlarda farklı reolojik kan akışı modellerinin uygulanmasının etkisini özetlemektedir. İnsan kan akışının evrensel olarak kabul edilmiş tek bir hesaplama modeli olmadığı için farklı yaklaşımlar araştırılmaktadır. Bu çalışmada, bir kapiler segmentin üç boyutlu eş odaklı mikroskop görüntüsü ANSYS Fluent kullanılarak modellenecek ve analiz edilecektir. Üç farklı model incelenmiştir: Newton modeli, Newton olmayan Carreau modeli ve ampirik ilişki. İlk model, segment boyunca sabit bir viskoziteye sahiptir. İkinci model, Carreau modeli kullanılarak kanın kesme incelmesi davranışını açıklamıştır. Son model de ise, kanın bağıl görünür viskozitesini tüp çapı ve kan hematokritiyle ilişkilendiren ampirik bir ilişkidir.

3D, sabit, laminer, tek fazlı Newtonian ve Newtonian olmayan akış modelleri, mikro damar segmenti boyunca kan akışını araştırmak için kullanılmıştır. Simülasyon

sonuçları, yukarıda bahsedilen modelleme yaklaşımlarını kullanmanın sonuçlarını anlamak için değerlendirilmiştir.

Modeller arasında gözle görülür bir fark sergilediği için basınç düşüşünün en önemli sonuç olduğu bulunmuştur. Öte yandan, modelin değiştirilmesinin hız ve girdap sonuçları üzerinde küçük bir etkisi vardır. Ayrıca hematokrit değerinin küçük bir yüzdeyle bile artırılmasının basınç düşüşünde gözle görülür bir artışa yol açtığı da fark edilmiştir.

Anahtar Kelimeler: Hesaplamalı Akışkanlar Dinamiği, kan reolojisi, Newton tipi akışkanlar, Newton tipi olmayan akışkan, kılcal damar, mikrosirkülasyon.

ABSTRACT

INVESTIGATING THE EFFECT OF DIFFERENT RHEOLOGICAL MODELS ON THE BLOOD FLOW IN CAPILLARY SEGMENTS

Masah Omar Mustafa ABUBAKER

Master's Degree, Department of Mechanical Engineering

Supervisor: Assoc. Prof. Dr. Özgür Ekici

Co-Supervisor: Assoc. Prof. Dr. Şefik Evren Erdener

December 2021, 89 pages

This study outlines the effect of applying different rheological blood flow models in capillaries. As there is no single, universally accepted computational model of the human blood flow, different approaches are investigated.

In this work, three-dimensional confocal microscopy image of a capillary segment will be modeled and analyzed using ANSYS Fluent. Three different models were investigated: Newtonian model, a non-Newtonian Carreau model and an empirical relation. The first model had a constant viscosity throughout the segment. The second model accounted for the shear thinning behavior of blood using the Carreau model. The last model was an empirical relation that relates the relative apparent viscosity of the blood to the tube diameter and the blood hematocrit.

The 3D, steady, laminar, single-phase Newtonian and non-Newtonian flow models are used to investigate the blood flow through the micro-vessel segment. The

simulation results are evaluated to understand the outcomes of using the aforementioned modeling approaches.

It has been found that the pressure drop was the foremost result as it exhibits a noticeable difference between the models. On the other hand, changing the model has a minor impact on the results of the velocity and vorticity. It was also noticed that increasing the hematocrit value, even by a small percentage, leads to a noticeable increase in the pressure drop.

Keywords: Computational fluid dynamics, blood rheology, Newtonian fluid, non-Newtonian fluid, capillary, microcirculation.

ACKNOWLEDGEMENT

There are many people whom I would like to thank for their contribution in this study. Foremost, I would like to start by presenting my immense gratitude to my supervisor Assoc. Prof. Dr. Özgür Ekici for his guidance. Your invaluable expertise and your timely recommendations had a significant effect in shaping the thesis. I am indebted to your continuous support with even the smallest of details throughout the study. Thank you for your inspiring patience and insightful feedbacks at any needed time.

I would like to also acknowledge my gratitude to the Institute of Neurological Sciences and Psychiatry as they provided the foundation of this study. In particular, I would like to present my sincere appreciation to Assoc. Prof. Dr. Şefik Evren Erdener as he had key contributions that were crucial in completing the thesis and making it a comprehensive biomechanical study.

My gratitude also extends to the members of my thesis examining committee. They generously allocated time to offer valuable comments toward improving this work. I would especially like to thank Prof. Dr. Murat Köksal. Your insights throughout the study were most appreciated as you have taught me more than I could give you credit for.

My sincere thanks must also go to my second family at Çukurova. You have been my greatest gift there. My great group of friends here, esp Mai. I am indebted to all your contributions throughout the study.

Lastly, my beautiful family without whom I would not have been able to complete this research, and without whom I would not have made it through my studies. I would like to thank my siblings for their continuous support and for always having my back. My parents, whose love, prays, guidance and unyielding support are always with me. I am forever indebted to them for giving me the opportunities and experiences that have made me who I am. To them I dedicate everything, including this degree.

TABLE OF CONTENTS

ABSTRACT iii

ACKNOWLEDGEMENT v

TABLE OF CONTENTS vi

LIST OF FIGUERS viii

LIST OF TABLES xi

LIST OF SYMBOLS AND ABBREVIATIONS xii

1. INTRODUCTION 1

2. LITERATURE REVIEW 4

2.1. Importance of Blood and Its Properties 4

2.2 Blood Vessels and Circulation of Blood 4

2.3 Properties of the Blood and Its Components 6

2.4 Microfluidics 10

2.5 Blood Rheology 11

2.6 CFD and Previous Studies 13

3. THEORY, MODELLING AND METHODOLOGY 16

3.1 Capillary Segment 19

3.2 Models 22

3.3 Blood Flow in the Capillary Segment 23

4. RESULTS AND DISCUSSION 26

4.1 Single-Phase Flow and Two Phase Flow 26

4.2 Results of the Empirical Relation Simulations 27

4.3 Comparison between the Models 28

5. CONCLUSION 42

6. REFERENCES 46

Appendix 55

App 1 – Tables 55
App 2 – Codes 62
App 3 - Thesis Originality Report 90
CIRRICULUM VITAE 91

LIST OF FIGUERS

Figure 3. 1: Five different cylinders with 6, 7, 8 and 9 μm in diameters and varying lengths that resemble the geometrys in Windes et al. [88]. 18
Figure 3. 2: a) The 3D confocal microscopy image of the capillary segment before processed, b) The processed segment.....21
Figure 3. 3: Mesh independency test results for different mesh structures. 21
Figure 3. 4: Processes used to utilize the varying viscosity along the segment 24
Figure 3. 5: a) Equally spaced planes placed along the capillary dividing it into 10, 20 and 30 sections equal in length, b) Capillary segment divided into 10, 20 and 30 section with varying length. 25
Figure 4. 1: The pressure drops of 6 simulations with equally spaced planes. Three of the simulations used the average value of the viscosity while the remaining half used linear correlations. 27
Figure 4. 2: The pressure drops of 6 simulations with planes placed at varying lengths. The average value of the viscosity was employed in three simulations, whereas linear correlations were used in the other half. 28
Figure 4. 3: The pressure contour along the capillary segment, (New) Newtonian model, (Car) Carreau model, (Emp40) empirical relation with H_t of 0.40 (Emp45) empirical relation with H_t of 0.45 29
Figure 4. 4: The velocity streamlines along the capillary segment, (New) Newtonian model, (Car) Carreau model, (Emp40) empirical relation with H_t of 0.40 (Emp45) empirical relation with H_t of 0.45 30
Figure 4. 5: The three sections along the segment chosen for further studies. 31
Figure 4. 6: The first section along the segment chosen for further studies.....31
Figure 4. 7: The pressure contour of the first section along the segment, (New) Newtonian model, (Car) Carreau model, (Emp40) empirical relation with H_t of 0.40 (Emp45) empirical relation with H_t of 0.45 31
Figure 4. 8: The velocity contour of the first section along the segment, (New) Newtonian model, (Car) Carreau model, (Emp40) empirical relation with H_t of 0.40 (Emp45) empirical relation with H_t of 0.45 32

Figure 4. 9: Vorticity contour of the first section along the segment, (New) Newtonian model, (Car) Carreau model, (Emp40) empirical relation with H_t of 0.40 (Emp45) empirical relation with H_t of 0.45 32
Figure 4. 10: The second section chosen for further studies. 33
Figure 4. 11: The pressure contour of the second section along the segment, (New) Newtonian model, (Car) Carreau model, (Emp40) empirical relation with H_t of 0.40 (Emp45) empirical relation with H_t of 0.45 33
Figure 4. 12: The velocity contour of the second section along the segment, (New) Newtonian model, (Car) Carreau model, (Emp40) empirical relation with H_t of 0.40 (Emp45) empirical relation with H_t of 0.45 34
Figure 4. 13: The vorticity contour of the second section along the segment, (New) Newtonian model, (Car) Carreau model, (Emp40) empirical relation with H_t of 0.40 (Emp45) empirical relation with H_t of 0.45 34
Figure 4. 14: The last section along the segment chosen for further studies. 35
Figure 4. 15: The pressure contour of the third section along the segment, (New) Newtonian model, (Car) Carreau model, (Emp40) empirical relation with H_t of 0.40 (Emp45) empirical relation with H_t of 0.45 36
Figure 4. 16: The velocity contour of the third section along the segment, (New) Newtonian model, (Car) Carreau model, (Emp40) empirical relation with H_t of 0.40 (Emp45) empirical relation with H_t of 0.45 36
Figure 4. 17: The vorticity contour of the third section along the segment, (New) Newtonian model, (Car) Carreau model, (Emp40) empirical relation with H_t of 0.40 (Emp45) empirical relation with H_t of 0.45 37
Figure 4. 18: The cross-sections chosen for further studies. The sections highlighted in orange have the highest viscosities, the sections highlighted in blue have the highest gradient in viscosity while the sections in pink have the lowest viscosities. 38
Figure 4. 19: Pressure contour of the different models at 6 different locations along the segment. The sections on the left-hand side have the highest viscosities, the sections in the middle have the highest gradient in viscosity while the sections on the right-hand side have the lowest viscosities. 38
Figure 4. 20: Velocity contour of the different models at 6 different locations along the segment. The sections on the left-hand side have the highest viscosities, the

sections in the middle have the highest gradient in viscosity while the sections on the right-hand side have the lowest viscosities. 40
Figure 4. 21: Vorticity contour of the different models at 6 different locations along the segment. The sections on the left-hand side have the highest viscosities, the sections in the middle have the highest gradient in viscosity while the sections on the right-hand side have the lowest viscosities. 40

LIST OF TABLES

Table 1: The results of single-phase flow compared with two-phase flow results..... 26
Table 2: Cross-sectional area, diameter and the viscosity obtained from 10 equally spaced planes placed along the segment with H_t of 0.45..... 55
Table 3: Cross-sectional area, diameter and the viscosity obtained from 20 equally spaced planes placed along the segment with H_t of 0.45..... 56
Table 4: Cross-sectional area, diameter and the viscosity obtained from 30 equally spaced planes placed along the segment with H_t of 0.45..... 57
Table 5: Cross-sectional area, diameter and the viscosity obtained from 10 planes placed at varying distances along the segment with H_t of 0.45 58
Table 6: Cross-sectional area, diameter and the viscosity obtained from 20 planes placed at varying distances along the segment with H_t of 0.45 59
Table 7: Cross-sectional area, diameter and the viscosity obtained from 30 planes placed at varying distances along the segment with H_t of 0.45 60
Table 8: Cross-sectional area, diameter, the constant C and the viscosity obtained from 30 planes placed at varying distances along the segment with H_t of 0.40..... 61

LIST OF SYMBOLS AND ABBREVIATIONS

Symbols

ρ	Density
t	*time*
ΔP	Change in pressure
D	Diameter
H_t	Hematocrit
l	Length
Q	Flow rate
μ	Viscosity
μ_{rel}	Relative viscosity
$\mu_\circ$	Zero shear viscosity
$\mu\infty$	Infinite shear viscosity
n	Power-Law index
λ	Time constant
$\dot{\gamma}$	Shear rate
C	A constant that describes the dependence of viscosity on H_t

Abbreviations and Acronyms

CFD	Computational fluid dynamics
New	Newtonian Model
Car	Carreau Model
Emp40	Empirical Relation Model with H_t of 0.4
Emp45	Empirical Relation Model with H_t of 0.45
UDF	User-Defined Function
CNS	Central nervous system
PBS	Phosphate buffered saline
App. No.	Approval number

1. INTRODUCTION

The circulatory system plays a plethora of important roles in sustaining life. These roles include but are not limited to, (i) distributing oxygen and nutrients to the tissues, (ii) removing metabolic byproducts, (iii) limiting the spread of infections and protecting against potential diseases, (iv) stabilizing the blood pH level, (v) regulating the body temperature, (vi) controlling the distribution of fluids, (vii) minimizing blood loss during injuries, (viii) contributing to tissue growth and blood vessel maintenance, etc [1]–[3].

The importance of hematology and the study of blood diseases cannot be overstated. Hematologists have made many poignant contributions to the health ecosystem [4]. Recent developments in hematology have been able to shed some light on new knowledge regarding bone disease, certain types of cancer, and other conditions. Hematology also has an indispensable role in diagnosing and treating infectious diseases [5], [6]. The ongoing COVID-19 pandemic has been instrumental in accentuating the essence of clinical hematology laboratories. These laboratories have opened up the possibility of diagnosing the infection, providing a prognosis of the course of the disease, and carefully outlining the adequate response to the treatment [7].

Developments in the rheological models shed light on the change of rheological properties of the blood and its components, particularly that due to pathological disturbances, which might be the main reason behind many cardiovascular-related disorders. Hence, being able to model and predict the rheological response of blood is of a great importance in understanding, diagnosing and treating these disorders [8].

This study investigates the effect of applying different rheological models on the blood flow in a capillary segment. 3D confocal microscopy images of capillary segments were obtained in collaboration with the Institute of Neurological Sciences and Psychiatry. The aforementioned images were processed using ANSYS 18.2 before being used in the simulations.

Computational fluid dynamics (CFD) is a vital discipline in developing and optimizing designs through computational simulations. That notwithstanding, its application in the biomedical field is only in the infancy stage. This is due to the complexity of human anatomy and fluid behavior. However, CFD has proven to be an indispensable tool in understanding the flow of blood in the human body. In addition, numerical simulation using CFD has also proven to be a useful tool in understanding flow physics, guiding experimental work, and interpreting available experimental data. The CFD software, Fluent, which was used in this study, is one of the most extensively used software. Its ability to solve the widest range of problems made it ideal for this research. Furthermore, the processing and post-processing tools provided by the ANSYS Fluent commercial package have the potential to help to describe and analyze the flow in the fluid domain.

In recent years, reams of published articles explored mathematical and computational models of blood flow; however, few of them validated or compared the results of the suggested models with a real flow. It should be noted that the majority of these articles investigated the macroscale flow. Thus, there is a need for accurate models of blood rheology to understand microcirculation.

Different models are used to investigate the effects of employing different rheological models on the capillary blood flow. Numerous results of published articles investigating rheological models were compared and analyzed. In the end, 3 different rheological models of blood flow in capillaries are chosen to be applied in this study. The 3D, steady, laminar, single-phase, Newtonian/non-Newtonian models are used to investigate the blood flow through the micro-vessel segment.

The capillary segment used in this study has a unique structure. To the best of the author's knowledge there has not been any segment used the literature with such an accurate illustration of the deviations present along the segment. Most of the published articles investigated the flow in cylinderical tubes or a rough approximation of the structure of the vessels.

The sections of the study are as follows; after the introductory chapter, the literature review is compiled in Chapter 2. The theory, modeling, and methodology are presented in Chapter 3. The chapter also contains the governing equations of the numerical solution, as well as, details about the geometry, mesh, and the proposed models. Chapter 4 states and compares the results of the simulations. Finally, the last chapter evaluates and summarizes the findings of the research.

2. LITERATURE REVIEW

2.1. Importance of Blood and Its Properties

Blood plays a major role in the overall health of the human body. This is predicated on the fact that it is the liquid medium responsible for carrying and sustaining the most basic elements of life [9]. For centuries, physicians have been certain of its importance to overall health. Many cultures hold the belief that blood is a symbol of both life and death.

Chinese physicians were known of being able to diagnose over 20 diseases and syndromes in various organs of the body by just examining one's pulse [10], [11]. According to Chinese medicine, the proper circulation of the blood depends on the temperature of the body, smoothness of the vessels, and interaction between the liver, spleen, heart, and lungs [12]. Over the last few hundred years, curiosity-driven research has been behind the development in hematology [5].

Blood plays an important role in nutrition, respiration, waste removal, internal communication, thermoregulation, and balance of water and acid in the human body [13]. The volume of the blood of a healthy adult ranges from 4 to 6 liters, which makes up about 7% of the body weight. Around 13% of that volume is found in the arteries, while nearly 7% is in the capillaries [8], [14].

2.2 Blood Vessels and Circulation of Blood

Blood vessels are a key component of the circulatory system. They play a major role in tissue morphogenesis, organ development, inflammation, wound healing, barrier formation, and elements transportation. Furthermore, understanding the structure and pathological alteration of the blood vessel plays a key role in understanding pathogenesis [15]. There are three main types of vessels; arteries, capillaries, and veins. The structure of these vessels varies depending on their position in the cardiovascular system [14].

Arteries and arterioles have thick walls and elastic fibers that help withstanding the high blood pressure. They are covered by smooth ring-shaped muscles that contract and relax to regulate the flow of the blood [16]. The regulation of blood flow input into the capillaries occur particularly at the level of precapillary; arterioles [17]. This input is distributed in an interwoven dense network of capillaries to match the needs of neurons and glia in the central nervous system (CNS). In CNS, capillaries possess a blood-brain barrier that tightly regulate the transportation of molecules between blood and parenchyma [18]. This barrier is composed of endothelial cells, basal lamina and surrounding astrocyte endfeet. The endothelial cells of this barrier are unique. They are continuously interconnected with tight junctions that limit the paracellular flux [18]. On the abluminal surface of endothelial cells, embedded in the basement membrane, pericytes with contractile capabilities are located [19]. Internal luminal surface of endothelial cells is coated with a glycoprotein layer, called glycocalyx that has important regulatory roles in capillary physiology [20]. This glycocalyx layer can cause a substantial increase in microvascular flow resistance, especially at low velocities [21]. All these elements make the capillaries very different from simple tubes, with highly dynamic constrictions, dilations and irregularities along the route. Further complicating the system.

Secomb et al. (2001) stated that an increasing flow velocity is accompanied by a decreased flow resistance and an increasing Fåhraeus effect. The increasing flow velocity also affects the shape of the RBCs in capillaries [22]. The pressure gradient along the vessels provides the force needed to overcome the resistance to the blood flow [23]. The flow in the arteries faces high resistance that helps control the blood pressure and decreases the downstream flow to the capillaries. As the blood flows through the arterioles, it faces a resistance and pressure drop in the vascular system [16]. It is worth noting that the capillary bed in the brain microcirculation is the site of largest hemodynamic resistance [24]. Although the flow in capillaries faces the highest pressure gradient, it only accounts for a small fraction of the total pressure drop in the circulatory system due to the short length of the capillaries [25].

The cycle of the blood continues as the capillaries merge into venules and then into veins that carry the blood back to the heart. The blood pressure at the entrance of the venules is very low compared to that at the entrance of arterioles. Since there is no need for the vessel walls to withstand high pressures, the venules and veins have thin walls. This is crucial to overcome the low pressure as well as the gravity effects to allow the return of the blood back to the heart.

Blood flow faces a lower pressure drop as it passes through the venules and veins due to their low resistance to the flow [16]. The vessels in the venous system have large diameters that facilitate the movement of the sluggish flow with low pressure drop. While the average blood pressure drops, the velocity of the blood increases as it enters the veins. Veins have skeletal muscle pumps and one-way valves to permit a unidirectional flow [26]. A small change in the pressure of the venous system, which contains up to 70% of the circulating blood, can mobilize the stored blood [16].

The blood traveling through the circulatory system flows through various types of vessels with changing diameters that affect the physical characteristics of the blood. Thus, different parts of the circulatory system require different flow modeling approaches to obtain a satisfactory result. For example, the blood can be modeled as a Newtonian fluid in large arteries. This is considered a good approximation, especially at high shear rates. However, it is not an accurate approach when dealing with the blood flow in small vessels [27], [28].

2.3 Properties of the Blood and Its Components

Viscosity represents the internal resistance of the blood to flow. This resistance is due to the frictional force between the layers that move relative to each other. As the blood flows through the vessel, the layers within the vessel move at different velocities. The fluid in direct contact with the wall assumes a zero relative velocity due to the no-slip condition [23].

Due to the shear force between the layers, the layer near the wall slows down the adjacent layer, which slows down the next layer, and so on. This phenomenon is responsible for the development of the velocity profile [29].

Blood is a shear-thinning fluid. This means that its viscosity decreases exponentially with increasing shear rates. Although cardiovascular specialists consider blood viscosity with values 3.5-5.5 cP to be normal, the viscosity of the blood cannot be characterized by a single value [30], [31]. Instead, it should be expressed as a function of shear rate, that depends on the rheological properties of the RBC that are affected mainly by the diameter of the vessel and the flow rate [31]. Blood may possess a viscosity of 5-6 cP at a shear rate of 200 s^{-1}, however, this viscosity may increase up to 60 cP at a shear rate of 0.1 s^{-1}. This is one of the reasons behind the fluctuating values of viscosity in circulatory system where the shear rate may vary from a few s^{-1} to over 1000 s^{-1} [30].

Blood has thixotropic and viscoelastic properties that affect the local hemodynamics. Both the blood and the walls of the vessels exhibit a viscoelastic behavior in a way that an elastic and viscous component transmits the stored and dissipated mechanical energy through the system [32]. While some papers model the wall vessels as an elastic wall many considered it to be rigid to simplify the solution. Eslami et al. (2020) examined the effect of the elasticity of the wall in the coronary arteries using hemodynamic numerical simulation. The paper showed that there is no difference between wall elasticity and rigid wall in the time average wall shear stress [33].

A thixotropic fluid has a time-dependent shear-thinning property. Where the viscosity of the blood is affected by the history of motion for a given shear/flow rate, the viscosity usually decreases with time [34]. The yield stress of blood ranges from 0.002 to 0.40 dynes/cm^2 depending on the rheometer and the experimental method used to measure it [13]. The yield stress is not constant through the circulatory system. It could be considered as a function of time as it depends on the thixotropy. The density of the blood is about 1050 kg/m^3, while its pH range is around 7.35-7.45 [8], [14].

The viscosity of the blood, which is typically 0.0035 Ns/m^2, can go up to 50 times higher when sickled cells are present [8], [35]. It could also be lower than the normal value for patients with severe anemia. The presence of sickled cells decreases the oxygen in the blood, increases the amount of oxygen transported from RBCs to the tissues, slows down the blood flow, and decreases the flow to the capillary. That is why modeling a healthy blood flow differs from the flow with sickled blood cells. The viscosity of the blood also depends on the hematocrit value, the viscosity of the plasma, and the mechanical properties of the RBCs [30]. Hematocrit (H_t) is the percentage of RBCs in the blood. The H_t range is not a constant value; it ranges over an interval. The normal H_t ratio for a healthy human is 42-54% for men and 36-48% for women [36]. An increase in the hematocrit value can lead to an increase in the blood viscosity at all the shear rates [31].

Formed elements constitute 40-45% of the blood. These formed elements are cells and cell fragments with definite structures enclosed in a membrane suspended in the plasma [16]. They include platelets, white blood cells (WBCs), and red blood cells (RBCs). Platelets are responsible for clotting to stop bleeding, while WBCs are responsible for immune responses. RBCs are mainly responsible for the transportation of O_2 and CO_2 in the blood [37]. Most of the cellular components in the blood have a brief lifespan as billions of these cells die every day. Thus, the continued production of formed elements in the bone marrow is vital for human survival [38].

A range of 45-60% of the volume of the blood consists of plasma; a medium in which the cellular components of the blood are suspended. Plasma is a clear, straw-colored liquid composed of about 90% water with over 100 different dissolved solutes including proteins. These proteins have a high molecular weight which prevents them from passing through the capillary walls. Plasma distinguishes the blood from the other connective tissues by enabling the elements to circulate throughout the body [38]. It acts as a lubrication layer between the blood cells and the vessel wall [39]. Plasma can be considered as a Newtonian fluid, however, the blood as a whole is mainly accounted for as having a non-Newtonian behavior particularly at low shear rates [38]. Many of the researches that were conducted over the past two decades modeled the blood as a

Newtonian fluid. However, in small vessels, the non-Newtonian effects are dominant. Hence, the blood is considered to be non-Newtonian [40], [41].

Red blood cells, also known as erythrocytes, are the densest cellular component of the blood. They account for around 95% of the formed elements and have the highest effect on the mechanical properties of blood [38]. Human RBCs have a basic biconcave-disk shape with a diameter of ~8 μm. In capillaries with diameters between 3 and 13 μm, RBCs can easily be deformed into a parachute-like shape due to external forces [42]. The shape RBCs take within the capillaries depends on several factors including the velocity of the flow, vessel diameter, cell geometry, RBC membrane characteristics, cytoplasmic composition, pressure gradient, and internal viscosity [31], [43]–[45]. At high shear rates, RBCs are deformed in a way that forces the cells to align parallel with laminar flow streamlines. This causes a decrease in the viscosity of the blood and the internal resistance of blood to flow. At low flow rates, RBCs lose their parallel alignment with the flow streamlines [31], [34]. In this case, RBCs take a biconcave disk shape that tends to form aggregates which leads to an exponential increase in the viscosity [46].

Deformability is a vital feature that enables RBCs to travel through even the smallest capillaries [44]. RBCs can pass constrictions or small capillaries with apertures much smaller than the size of their cross-section [47]. In the smallest capillaries, RBCs flow in a single file (bolus flow). The bolus flow is not very stable at D = 8 μm. In fact, the RBCs may show some clustering in the capillaries under this condition. As the vessel diameter increases to D=10 μm, RBCs display a more stable single-file motion. However, when the vessel diameter is further increased to D=12μm, a hematocrit-dependent transition from single-file to multi-file flow is observed. In this case, single-file and multi-file motions may coexist [48], [49]. In a large vessel, the deformable RBCs are concentrated near the axis of the vessels, while platelets and WBCs are near the wall [50].

The cellular elements of the blood interact with each other and with the vessel wall. RBCs prompt the radial motion of the WBCs toward the wall. The migration of WBCs is affected by the shape of the RBCs. Flat RBCs can easily aggregate and form a shape of rouleaux under low shear conditions [51]. This provides the WBCs with

sufficient force to start rolling on the endothelium. The net force applied to the bouncing WBCs fluctuates from positive to negative as they roll on the wall of the vessel.

The rouleaux formation is a reversible low-energy process. RBCs that aggregate to form the rouleaux may disaggregate at regions with high shear rates such as arteries [31], [51]. A rouleaux with ellipsoidal RBCs, on the other hand, applies lower force on the WBCs. This is because RBCs are inclined to roll against one another, thus the rouleaux dissociates faster. At a low shear rate, another problem arises in vessels due to the non-homogeneous distribution of RBCs. Phase separation and particle migration near the boundaries are higher in capillaries compared to the larger blood vessels. Therefore, to find the true viscosity of the blood, a data reduction process must be performed unless a constitutive model of the blood is priory made. On the other hand, the viscosity at a higher shear rate is practically constant [13]. The difficulty in finding some measurements in capillaries might be the reason behind the low number of papers published that relate modeling at microscale compared to the macroscale blood flow.

2.4 Microfluidics

Microfluidics is a science that handles and analyzes the behavior of fluids at the micrometer scale [52]. Due to the small size of the system in question, the behavior of the fluid differs from the conventional flow [53]. This field caught the attention of many researchers after the end of the cold war [54]. Microfluidic systems were designed and used to detect biological and chemical threats. Microfluidics was also considered a promising technology in the 3-billion-dollar Human Genome Project, where there was a need for systems with high sensitivity and resolution [55], [56].

Over the past two decades, there has been significant progress in the field of microfluidics [55]. This progress led to the creation of many devices with smaller volumes, shorter reaction times, high sensitivity, and the possibility of parallel operation [52], [54]. There have been many devices manufactured that were capable of outperforming their normal-sized versions. This is due to the different forces that dominate at the microscale [55]. Although gravity may be one of the dominant forces at

the macroscale, it has a lower effect at the microscale when compared to diffusion, surface tension, and the resistance of the fluid. It is also important to note that due to the small size of channels at this scale, the flow is almost always laminar. This means that the streamlines adjacent to each other will not mix except by diffusion [52], [55]. The mixing takes place between two streams transverse to the direction of flow. Utilization of this characteristic resulted in the creation of many devices including blood diagnostics, microfluidic circuit boards, in-channel microfabrication, and DNA analysis devices, just to name a few [57].

Reynolds number is a dimensionless quantity that correlates the ratio of the inertia forces to the viscous forces. At low values, the flow is considered laminar. Inertia force is considered trivial and the flow is controlled almost entirely by the viscous force and pressure [27]. As the value increases, the flow undergoes a transition from laminar to turbulent [58]. Blood flow for a healthy human is normally considered laminar. However, it may have high-frequency fluctuations that indicate turbulence. Blood is a suspension of mainly RBCs. The concentration and size of the RBCs appear to hinder the formation of eddies [59]. However, some diseases may affect the nature of the flow. For example, high blood pressure causes an increase in velocity which increases Reynolds Number thus increasing the chances of turbulent flow [60]. Other factors that may affect the nature of the flow include dynamical relaxation parameters, diffusion, and perfusion [59].

2.5 Blood Rheology

The development of new techniques used to study the behavior of blood flow has led to many advancements in blood rheology [61]. Rheology is the study of the deformation and flow of matter due to the forces applied [62], [63]. Hemorheology, on the other hand, is the application of the science of rheology to the blood and its components. Hemorheology of the blood is affected by the alterations of hematocrit ratio, cytoplasmic viscosity, plasma protein composition, vascular properties, RBC properties, etc [61].

Abnormalities in hemorheology indicate inadequate circulatory function of the system. There are many pathologies of hematological origin; some of these include thalassemia, leukemia, and anemia. Other hemorheological deviations may increase the risk of hypertension, diabetes, or even strokes. Consequently, understanding the various alterations of hemorheological parameters of the blood provides an insight to the underlying condition [38], [61].

Fluids may be classified under two main groups; Newtonian and non-Newtonian. Newtonian fluids have a constant viscosity which is independent of the shear rate. The shear rate of the Newtonian fluids is directly proportional to the shear stress, and its viscosity is only dependent on temperature [64]. On the other hand, the viscosity of the non-Newtonian fluid is dependent on the variations in shear rate or deformation history. Blood demonstrates a non-Newtonian shear-thinning behavior. This means that its apparent viscosity decreases as the shear rate of the blood increases [61].

In the circulatory system, the interactions between the cells and the wall play a significant role in the flow. Since the blood cells are not uniformly distributed, there has been a need for a type of measurement that would account for the effects of the rheological properties. Therefore, the apparent viscosity is used to represent the resistance to the flow, while accounting for the interaction of the blood components and the boundaries of the flow [27], [65].

Up till now, there is no universally used viscous model for the blood [66]. Some constitutive models for the non-Newtonian blood have been found. The Power-Law, Casson, Herschel-Bulkley, and Carreau-Yasuda are some of the models that show the shear-rate dependency of the viscosity [62]. Carreau has been chosen by many researchers for its accuracy compared to the other methods, as it gives one of the best approximations to the empirically measured blood viscosity compared to the previously mentioned non-Newtonian models.

2.6 CFD and Previous Studies

Over the years, CFD proved to be an indispensable tool in understanding the human body's fluid flow, particularly the blood flow and its rheological properties. According to rheologists, blood can be considered as a solid-liquid suspension or a multiphase liquid.

The choice of the approach to be used to model the flow of blood in the capillary depends on the complexity of the application. Chen et al. (2021) compared the single-phase and multiphase flow of cavopulmonary connection structures to evaluate the hemolysis risk. The multiphase flow simulation was able to display the mechanical behavior of RBCs and WBCs. The researchers found that the impact shear stress in the complex multiphase flow was smaller relative to that of the single-phase [67].

Fedosov et al. (2010) modeled the blood as a suspension of RBCs in microvessels of 10-40 μm in diameter. He used the dissipative particle dynamics method to model the blood flow with H_t ratio that ranges from 0.15 to 0.45. The paper explained that an increase in H_t values results in an increase in the blood's resistance to flow, as well as, the bluntness of the velocity profiles [68].

Botkin et al. (2019) proposed a formula for the resistance of the blood flow accounting for the hematocrit level. These researchers modeled the blood flow in a computer-generated microvessel network. The diameters of the vessels were below 10 μm. In the study, two approaches were used to mathematically model the RBCs motion. The first approach was of a two-phase continuum blood flow. A high viscosity was assigned to the RBCs that travel through the center of the vessel as a continuum flow. Conversely, the plasma had a much lower viscosity, as it surrounds the RBCs near the wall. The other approach was a discrete model of the blood flow where a single file of RBCs flows, and the effect of each RBC is considered. In this model, the plasma fills the spaces between the RBCs, in addition to the space between the wall and the RBCs [39].

Some of the numerical methods that were used to capture the behavior of RBCs include; the boundary element method (BEM), direct numerical simulations (DNS), and lattice Boltzmann method (LBM). In BEM, the mesh is generated on a 2D surface, even though the flow is 3D; hence, the total number of meshes is lower than that in the other methods. It is considered a good tool in the analyses of blood flow with moving boundaries. Cristini and Casab (2003) used adaptive meshing techniques to analyze the motion of RBCs at the microscale level [69]. LBM is also a numerical method used in CFD where the working fluid is represented by an assembly of virtual particles. This enables the modeling of a multiphase flow (i.e. blood flow) by introducing particular forces among the virtual particles that represent the RBCs. Some of the research that used LBM considered the blood to be Newtonian fluid [70], [71]. Others, however, modeled it as a three-phase non-Newtonian fluid [72].

Direct numerical simulations (DNS) is another numerical method used in modeling a multiphase blood flow. It is the most accurate approach used in simulating turbulent flows [73]. Although it is in its infancy, DNS has been considered an effective tool in examining complex multiphase flows. It can be used with laminar and turbulent flow applications. However, it is considered a very expensive method. This is because the computational capacity it requires predates that of conventional computers. The first DNS of a 3D cellular-scale blood flow in realistic microvascular networks was conducted in 2017 [74]. The unsteady flow was computed for a system small enough to enable the full solution of the application yet, not too large to capture trivial scale interactions [75].

The finite element method (FEM) is used to solve partial differential equations representing conservation laws by subdividing the domain into elements that form a grid. This method is usually used in the structural analysis of solids. It can be applied to fluids, but the model must be carefully formulated to ensure a conservative solution [76]. FEM is more stable than the finite volume method [77]; nevertheless, it may require more memory and provide a slower solution compared to FVM. Most of the research that was conducted using FEM modeled the blood as a Newtonian fluid [78]–[80]. Weddell et al. (2015) investigated the differences in the wall shear stress between non-Newtonian and Newtonian models [63]. While Mubita et al. (2014) used a multiphase non-Newtonian FEM model [81].

The finite volume method (FVM) is a widely used numerical approach in flow simulations. In this method, the governing equations are integrated over a volume or cell assuming a piecewise linear variation of the dependent variables (u, v, w, ƒ, T). The piecewise linear variation determines both the accuracy and the complexity of the solution [82]. The flux through the control volume in FVM is conserved making it a preferred method in CFD. This method can be used in various problems, including high Reynolds number turbulent flows, due to its advantageous memory usage and speed [83]. This made FVM a suitable choice for several fluid flow applications involving mass and heat transfer [83] .

Shibeshi and Collins (2005) investigated the hemodynamics of the blood flow using: Casson, Carreau and the power law models. Carreau model had the highest viscosity at all shear ranges. The power law model faced its lowest viscosity at a high shear rate while the Newtonian model faced it at a low one. At high shear rates, the Carreau model results coincided with the results of the Newtonian and Casson model. Yet, at low shear rates, the results coincided with that of the power law. It is also noteworthy to mention that Carreau model produced the smallest vortices while the Newtonian model produced the largest [84].

Many numerical approaches could be used to model blood flow. Choosing the right approach is important for an accurate and realistic simulation. Many researchers used a two-phase flow simulation of the blood vessels, taking into consideration the effect of RBCs and plasma. Some others opted to investigate the modeling of a three-phase flow simulation [67], [72], [81]. However, in this study, we are trying to investigate different models that will allow a reliable prediction of the blood flow without the need to simulate the motion of individual RBCs.

3. THEORY, MODELLING AND METHODOLOGY

In this chapter, different approaches are introduced to investigate the blood flow in a capillary segment. ANSYS Fluent is used in the computational process. Details of the computational processes including; domain, mesh, governing equations, boundary conditions, assumptions, etc. are available in this section.

The FVM is considered a powerful tool in modelling single-phase blood flow, especially in macrocirculation. However, there are a few limitations in analyzing multiphysics problems with moving boundaries especially at the microscale blood flow. Thus, in order to simplify the model the walls of the vessels are assumed to be rigid.

There are numerous mathematical models and engineering correlations that may be used to describe the movement of fluids. Nevertheless, there are two main conservation equations that FLUENT solves for every flow simulation; mass Eq. 1 and momentum Eq. 2 [85].

$$\frac{\partial \rho}{\partial t} + \frac{\partial \rho u_i}{\partial x_i} = 0 \tag{1}$$

$$\frac{\partial \rho u_i}{\partial t} + \frac{\partial \rho u_i u_j}{\partial x_j} = \frac{\partial p}{\partial x_i} + \frac{\partial}{\partial x_j}\left[\mu\left(\frac{\partial u_i}{\partial x_j} + \frac{\partial u_j}{\partial x_i}\right)\right] \tag{2}$$

The principles of mass and momentum conservation govern the motion of a fluid. The mass continuity equation, which is the differential form of the mass conservation, states that a region will conserve its mass in the absence of mass sources and sinks [86]. The momentum equation, on the other hand, states that the sum of the surface forces acting on an element of fluid is equal to the acceleration or rate of change of momentum [87].

In our simulations the flow is incompressible thus the density is constant. Accordingly, the mass and momentum conservation equations can be rewritten as follows:

$$\frac{\partial u_i}{\partial x_i} = 0 \tag{3}$$

$$\rho \frac{\partial u_i u_j}{\partial x_j} = \frac{\partial p}{\partial x_i} + \frac{\partial}{\partial x_j}\left[\mu\left(\frac{\partial u_i}{\partial x_j} + \frac{\partial u_j}{\partial x_i}\right)\right] \tag{4}$$

Three different modelling approaches were elected to be applied to the three-dimensional confocal microscopy images. However, before applying the various models to the segment, investigation of a recent two-phase flow study was made. This was performed to enable the comparison of the results obtained from a single-phase flow with those from the published article. The model of the recent study was applied to circular microchannels of various lengths and diameters.

The work published by Windes et al. in 2016 [88] was taken as a reference to investigate the difference that could arise from using a one-phase blood flow in the capillaries. Windes et al., [88] used standard second-order FVM to model the incompressible human blood flow through a cylinder. The three-dimensional, two-phase CFD model was composed of 3-7 RBCs placed in plasma. A relatively constant pressure drop across RBCs was observed. The results of viscosity and hematocrit of the model were compared with experimental data. The two-phase capillary flow model was validated for 5–10 μm diameters, 0.1-5 mm/s average flow velocities and up to 0.45 discharge hematocrits which is very similar to our simulations.

Equation 5 was used to find the relative apparent viscosity μ_{rel} (the ratio of apparent viscosity to suspending medium viscosity). Five different cylinders with varying length were modelled Fig.3.1. The length of the cylinders were chosen to resemble those of Windes et al. [88].

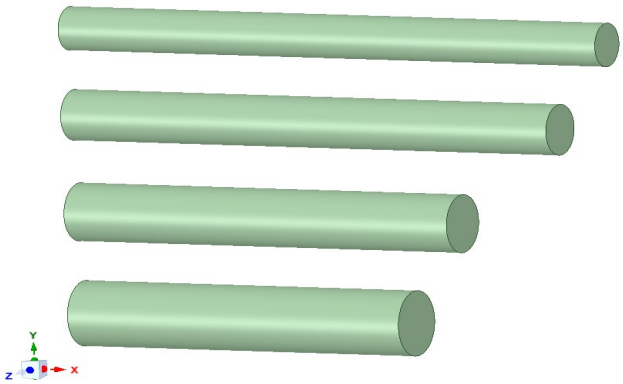

Figure 3. 1: Five different cylinders with 6, 7, 8 and 9 μm in diameters and varying lengths that resemble the geometries in Windes et al. [88].

The flow setting of the 3D microchannel blood flow included; no slip boundary condition and constant viscosity obtained from Eq. 5. The inlet boundary condition of the laminar flow had a fully-developed parabolic velocity profile set normal to the inflow velocity. The average inlet velocity was 0.5 mm/s and the vessel walls were assumed to be rigid. The outlet boundary condition was set to be zero gauge pressure. Outflow was also set as the outlet boundary condition in order to compare the results of the different exits. The density was set to 1050 kg/m^3 and the convergence criterion was chosen to be 10^{-6}.

$$\mu_{eff} = \frac{\Delta P}{l}\frac{\pi D^4}{128Q} \tag{5}$$

In the aforementioned simulations, an additional length was added to all the geometries to create a fully-developed parabolic velocity profile at the inlet. Although in a realistic model of the blood flow the velocity will not be fully developed due to the irregular shape of the vessels and the pulsatile nature of the flow. Yet, Windes et al. [88] used fully-developed velocity profile as an inlet boundary condition of the cylinder. In order to enable an accurate comparison, identical inlet boundary conditions were implemented in the cylinders' simulations. Since the flow is assumed to be steady and fully developed at the inlet, there will be no acceleration through our region of interest.

It is well-known that the pressure drop in the fully-developed region is lower than that in the developing region. This is mainly because the wall shear stress is at its highest at the hydraulic entrance region. It decreases gradually until it reaches to the fully developed region value. At the fully developed region, the shear stress becomes a linear function of the radial coordinate and remains constant along the flow direction [29], [89].

3.1 Capillary Segment

Three-Dimensional confocal microscopy images of capillary segments were obtained in collaboration with the Institute of Neurological Sciences and Psychiatry. The confocal microscopy image, also known as confocal laser scanning microscopy (CLSM), was used in the 20^{th} century to overcome the limitation of acquiring the subsurface image of turbid samples at a microscopic scale. Later on this technology was used on a wider range of applications [90].

Methanol-fixed retina, obtained from Swiss-Albino mouse samples, was used for the acquisition of the capillary segment images. These images were already available for another project. The procedure to obtain the images was approved by the Hacettepe University Animal Experimentation Local Ethics Board, App. No. 2018/20. There has not been any additional test carried out for the current study. Hence no additional procedural approval was required.

Capillary endothelial lining was labeled by incubating the whole-mount retina in fluorescein-conjugated tomato lectin (1:200 concentration) at +4 °C overnight. The samples were then washed in phosphate buffered saline (PBS), embedded in glycerol with Hoechst 33258 solution, and cover-slipped for imaging.

The process of taking the images was performed with a Leica SP8 laser scanning confocal microscope. Fluorescence was caught in the images with laser excitation at 405nm and 488 nm for Hoechst and fluorescein, respectively. A 63X oil immersion objective (NA: 1.4) was also used. A 40x40 μm image of the capillary segment with 512x512 pixels was obtained.

This image was obtained for a Z-stack of 11 μm with 0.3 μm Z-steps. Afterwards, it was converted to an isotropic Z-stack of 0.08 μm pixel resolution. The segment was then used for manual segmentation of the capillary lumen in Slicer3D software. In this process the endothelial lining was used as an outline. The segmentation was then exported in .stl format for further processing.

The .stl format segment obtained from Institute of Neurological Sciences and Psychiatry was processed using SpaceClaim before being used in the simulation. The segment with the unique structure displays the smallest deviations along the segment including the contractions and expansions. The 3D confocal microscopy of the segment had millions of sharp-edged facets that made it difficult to be handled using ANSYS Fig.3. 2a. Thus, there was a need to smoothen the geometry. This was accomplished by merging the facets along the segment. The edges of the inlet and outlet were first cut to straighten the inlet and outlet. The sharp inlet and outlet edges were a practical choice that facilitated the merging operation.

Small number of adjacent visible facets were chosen for each process. A range of 100-2500 facets were merged at a time to avoid any error or disfiguration of the segment. The merging process resulted in 45 patches along the segment. After the merging process, scaling operation was performed to the segment. This resulted in a segment with a length of around 131 μm and a varying cross-sectional area of 2-9 μm in diameter. The resulted segment is shown in Fig. 3.2b.

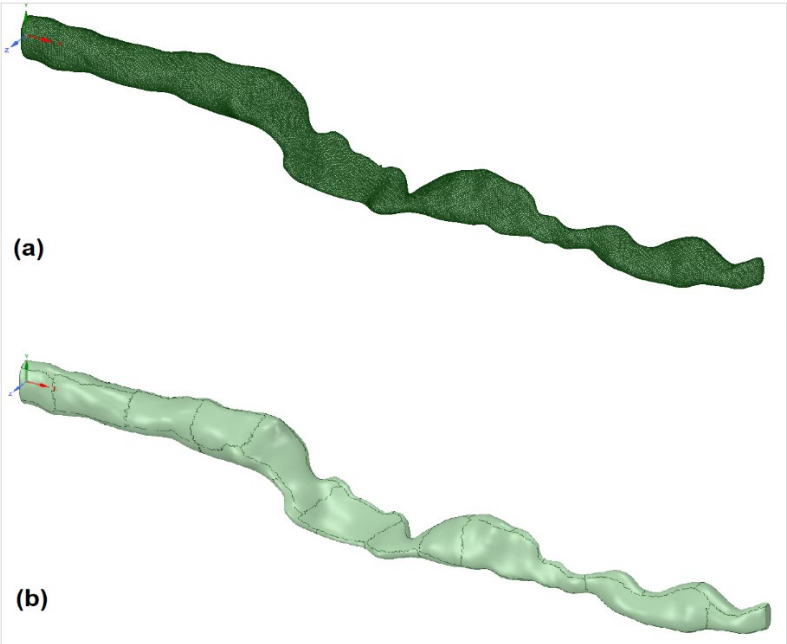

Figure 3. 2: a) The 3D confocal microscopy image of the capillary segment before processed, b) The processed segment.

After processing the segment, a mesh independence study of the Carreau model was performed to ensure a mesh independent results are obtained. Element sizes of 0.25, 0.2, 0.18 and 0.163 µm were used to find the optimal element size that would best represent the flow while using minimal computational recourses without a significant loss in accuracy Fig 3.3. The optimal mesh element size was around 0.18 µm.

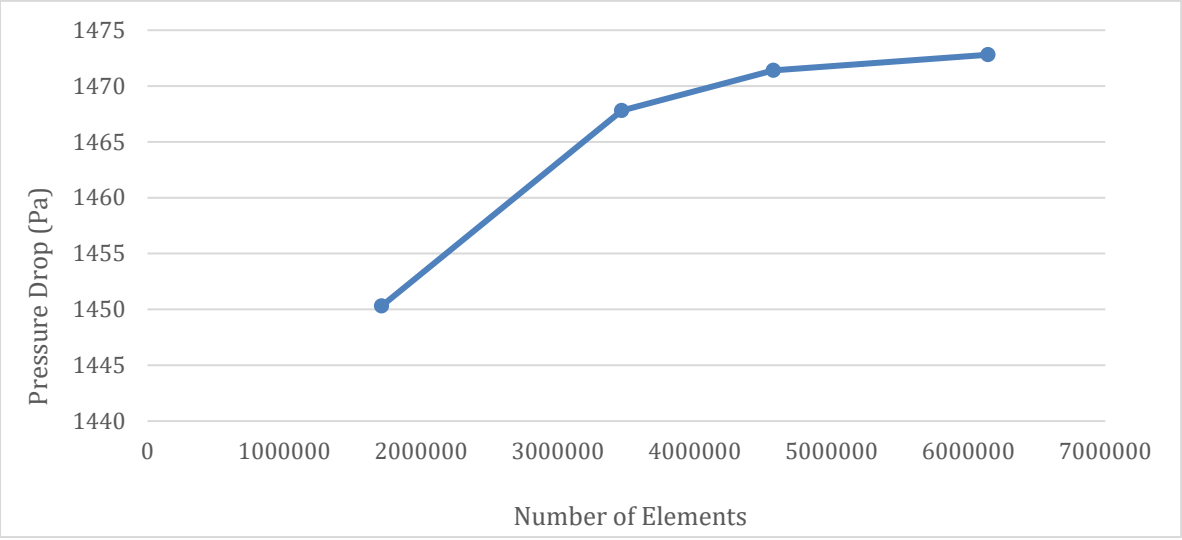

Figure 3. 3: Mesh independency test results for different mesh structures.

3.2 Models

The first applied model to 3D confocal microscopy image was non-Newtonian blood model. Carreau, Casson and the power law models are the most widely used non-Newtonian models [6]. These models have been chosen by many researchers for their accuracy compared to the other methods as they give a good approximation to the empirically measured blood viscosity. In our simulation, the shear thinning behavior of blood was accounted for by using the 'Carreau' model with the following blood properties [84].

Density (kg/m^3) ρ	1050
Time constant (s) λ	3.313
Power-Law Index n	0.3568
Zero Shear Viscosity (kg/m.s) $\mu_\circ$	0.056
Infinite Shear Viscosity (kg/m.s) $\mu\infty$	0.0035

In the Carreau model the viscosity of the fluid is calculated using the following equation [85]:

$$\mu_{eff} = \mu_\infty + (\mu_\circ - \mu_\infty)[1 + (\lambda\Upsilon)^2]^{\frac{n-1}{2}} \quad (6)$$

The second model was the Newtonian model with a constant dynamic viscosity of 0.0035 Pa.s, corresponding to a hematocrit value 0.43 [91]–[93]. This model was used in many researches that investigated the blood flow at a macroscale [78], [84], [91], [94]–[97]. The last investigated model in this study was an empirical equation proposed in 1992 by Pries et al., [98]. The developed correlation relates the relative apparent viscosity of the blood to the tube diameter and the blood hematocrit Eq. 7-9. Apart from for the viscosity, the domain and the flow settings were identical to the previous models.

$$\mu_{rel} = 1 + (\mu_{0.45} - 1)\frac{(1 - H_t)^C - 1}{(1 - 0.45)^C - 1} \quad (7)$$

$$\mu_{0.45} = 220\exp(-1.3D) + 3.2 - 2.44\exp(-0.06D^{0.645}) \quad (8)$$

$$C = (0.8 + \exp(-0.075D))(-1 + (1 + 10^{-11}D^{12})^{-1}) + (1 + 10^{-11}D^{12})^{-1} \quad (9)$$

In the aforementioned equations, D is the diameter in μm and $\mu_{0.45}$ is the viscosity that corresponds to the H_t value of 0.45.

3.3 Blood Flow in the Capillary Segment

Although there are numerous articles that investigated the flow in the blood vessels, only a few of them investigated the flow in the capillaries. Even fewer articles investigated the flow in a realistic domain rather than an approximation of the geometry, mainly a cylinder. In this section, the three previously mentioned models will be used to investigate the blood flow in the 3D confocal microscopy image of a capillary segment.

The Carreau model and the Newtonian model with constant viscosity were first applied to the segment. The flow setting of the 3D confocal microscopy image blood flow included; no slip boundary condition and the vessel walls were assumed to be rigid. The inlet boundary condition of the flow had constant inlet velocity of 0.5 mm/s set normal to the inlet. In these simulations two different outlet boundary condition; outflow and zero pressure gauge, were used in order to compare the results of the different exits. The density was set to 1050 kg/m^3 and the convergence criterion was chosen to be 10^{-6}. A Pressure-based, simple second order solver is used in FLUENT.

The last model applied was the empirical relation. In this model Eq. 7-9 were not directly implemented. This was due to the lack of means that could directly utilize the diameter of the segment. Thus, the following processes took place in order to implement the varying viscosity along the segment.

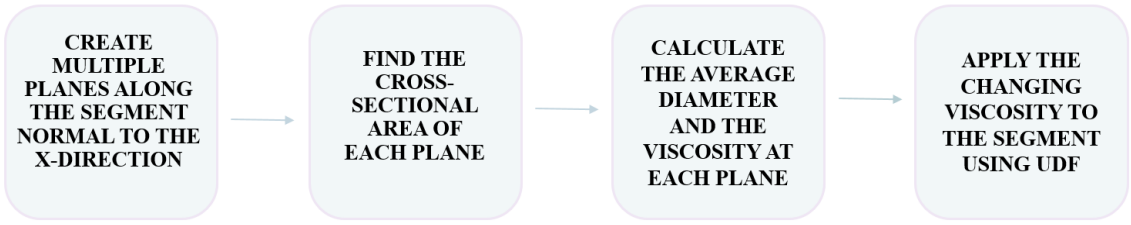

Figure 3. 4: Processes used to utilize the varying viscosity along the segment

Equally spaced planes were placed along the capillary segment dividing it into 10, 20 and 30 sections equal in length Fig. 3.5 (a). Afterwards, the segment was again divided into 10, 20 and 30 sections, however, the planes were not equally spaced. The planes were placed where there was the greatest variation in the geometry diameter and the viscosity value. This resulted in a capillary segment that had sections with varying lengths Fig. 3.4 (b).

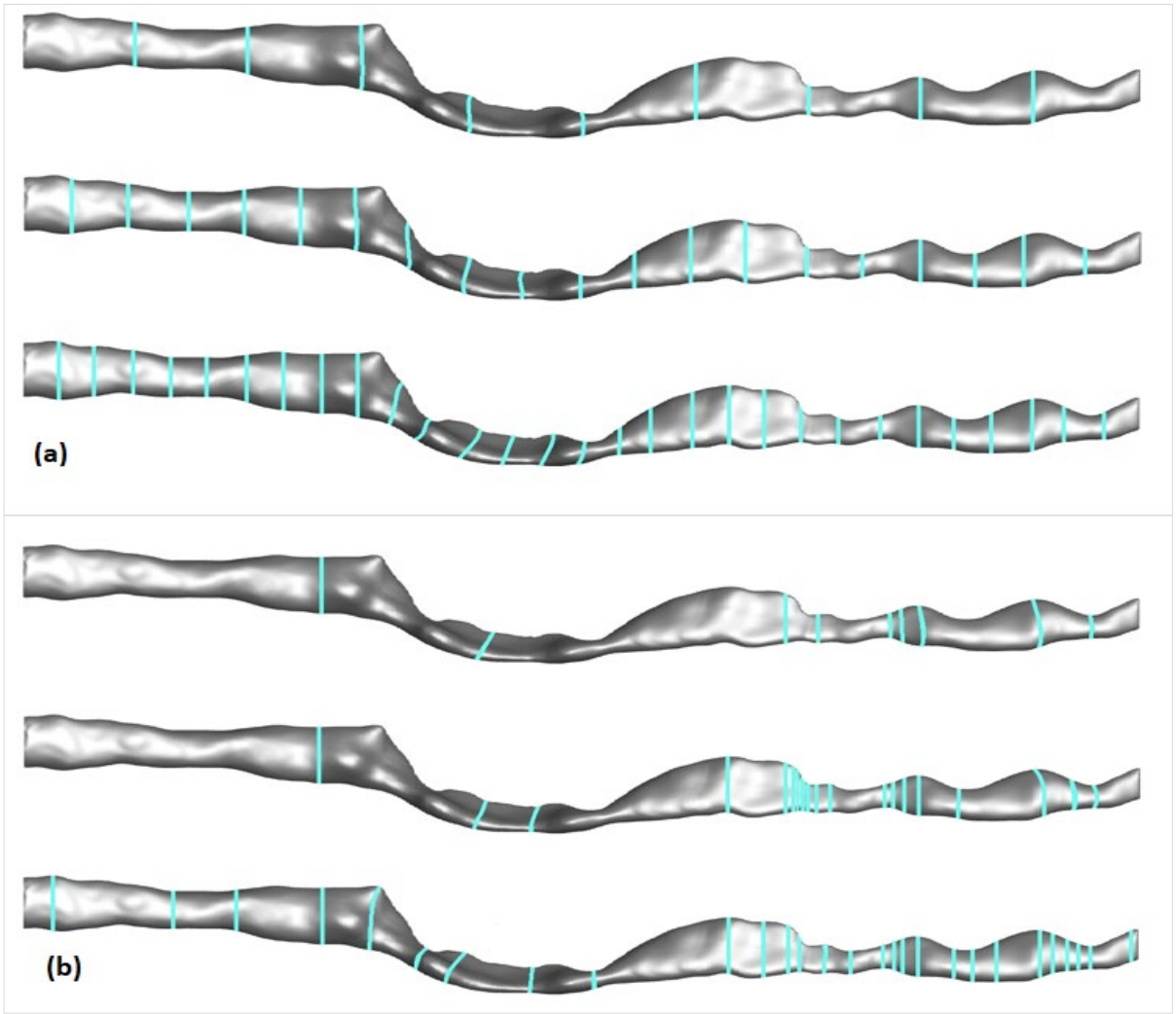

Figure 3. 5: a) Equally spaced planes placed along the capillary dividing it into 10, 20 and 30 sections equal in length, b) Capillary segment divided into 10, 20 and 30 section with varying length.

Twelve different simulations were conducted with six different section configurations. The first six simulations assigned a constant viscosity for each section. The average viscosity of two planes, at the beginning and the end of each section, was assigned to the flow in between the planes. In the remaining simulations, a linear correlation was assigned for each section utilizing the viscosity of the planes at the ends of each section.

Aside from the viscosity the previous simulations all had the same flow settings and hematocrit of 0.45 to enable a comparison between the results. One of the twelve simulations will be chosen as specimen for further examination.

4. RESULTS AND DISCUSSION

In this study, Newtonian and non-Newtonian fluid simulations of the blood flow have been conducted. First, the results of a single-phase flow are compared with the numerical study of Windes et al. [88]. The results of the empirical relation simulations are compared. Accordingly, one of the 12 simulations is chosen for further examination. Furthermore, the effect of changing the hematocrit ratio is investigated. In the end, a comparison between the models is presented.

4.1 Single-Phase Flow and Two Phase Flow

In the current study, there was a need to investigate the difference that could arise from using one-phase instead of a multi-phase blood flow. The numerical study published by Windes et al. in 2016 [88] was taken as a reference to investigate such a difference of flow in the capillaries. Five different cases were investigated.

The outlet boundary condition was set to be zero gauge pressure in the first set of simulations. Outflow was also set as the outlet boundary condition. The pressure drop obtained from setting the outlet boundary condition to zero gauge pressure was essentially the same as setting the outflow.

Table 1: The results of single-phase flow compared with two-phase flow results

Diameter (µm)	Length of the Segment (µm)	Apparent Viscosity (mPa.s)	Pressure Drop of the Two-Phase Flow reported by Windes [88]	Pressure Drop found by Single-Phase Flow (Pa)
6	72	1.575	50.4	50.3
7	65.1	1.68	35.55	35.7
8	51.3	1.785	22.89	22.9
9	44.4	1.838	16.1	16.13

The results of the performed simulations, available in Table 1, were almost identical to those found by Windes et al., [88]. Thus, a single-phase flow was chosen for modeling the segments.

4.2 Results of the Empirical Relation Simulations

Three different models were used in this study. One of these models is an empirical relation proposed by Pries et al., [98]. The correlation relates the relative apparent viscosity of the blood to the tube diameter and the blood hematocrit. Twelve simulations were conducted using the aforementioned correlation. For the first half of these simulations, planes were planted uniformly along the segment. The other half, on the other hand, had planes placed at various distances along the segment. The pressure drop results of the 12 simulations are present in charts 4.1 and 4.2.

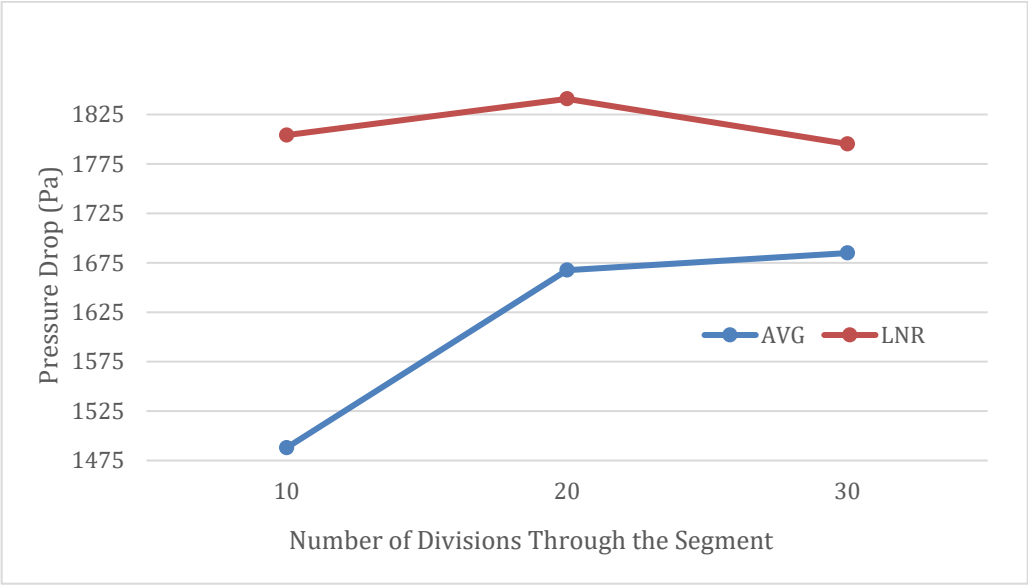

Figure 4. 1: The pressure drops of 6 simulations with equally spaced planes. Three of the simulations used the average value of the viscosity while the remaining half used linear correlations.

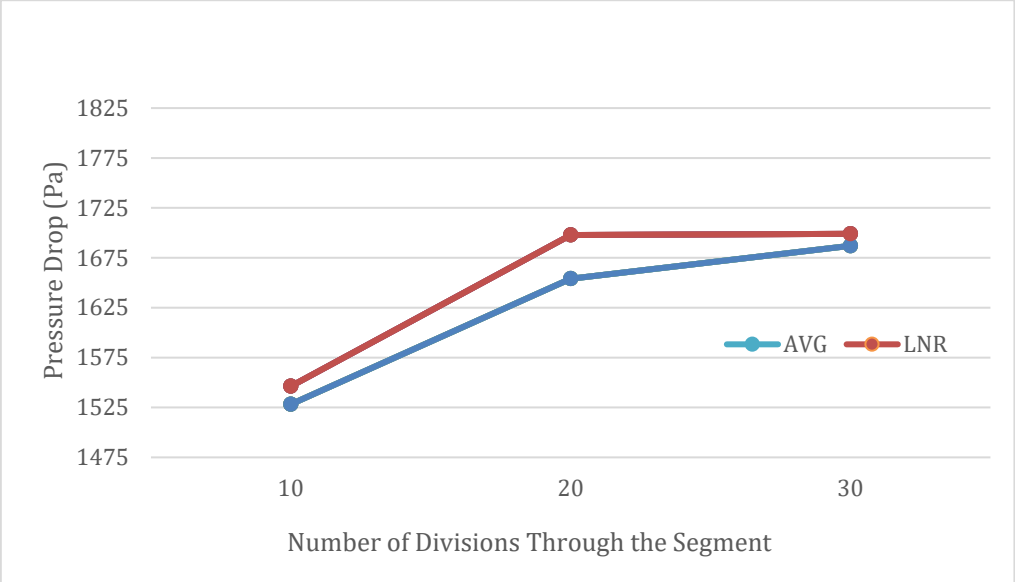

Figure 4. 2: The pressure drops of 6 simulations with planes placed at varying lengths. The average value of the viscosity was employed in three simulations, whereas linear correlations were used in the other half.

In the light of the previous results, the simulation of the evenly spaced planes showed a huge difference between the average and linear correlation results. Although an increase in the number of planes gave better results, the second set of simulations was considered more promising. The last simulation with linear correlation for 30 planes placed at varying lengths was chosen for further studies.

The aforementioned 12 simulations had a hematocrit of 0.45. In order to investigate the effect of changing the hematocrit, the UDF of the chosen simulation was modified. After adapting the UDF to the hematocrit of 0.4, the results were compared.

4.3 Comparison between the Models

In this section, we will take a closer look at the results of 4 different simulations. The first model was the Newtonian model with a constant viscosity of 0.0035 Pa.s along the segment. The second model was the Carreau model. The last two simulations used the aforementioned empirical relation with hematocrit of 0.40 and 0.45 respectively.

The four simulations' pressure, velocity, and vorticity findings are compared. Figure 4.3 illustrates the pressure contour along the capillary segment while Fig 4.4 presents the streamlines of the four cases.

Although there is no noticeable difference in the streamlines Fig 4.4, the empirical relation with H_t of 0.45 has a little bit higher velocity compared to the other models. The pressure contour, on the other hand, shows a great difference between the models.

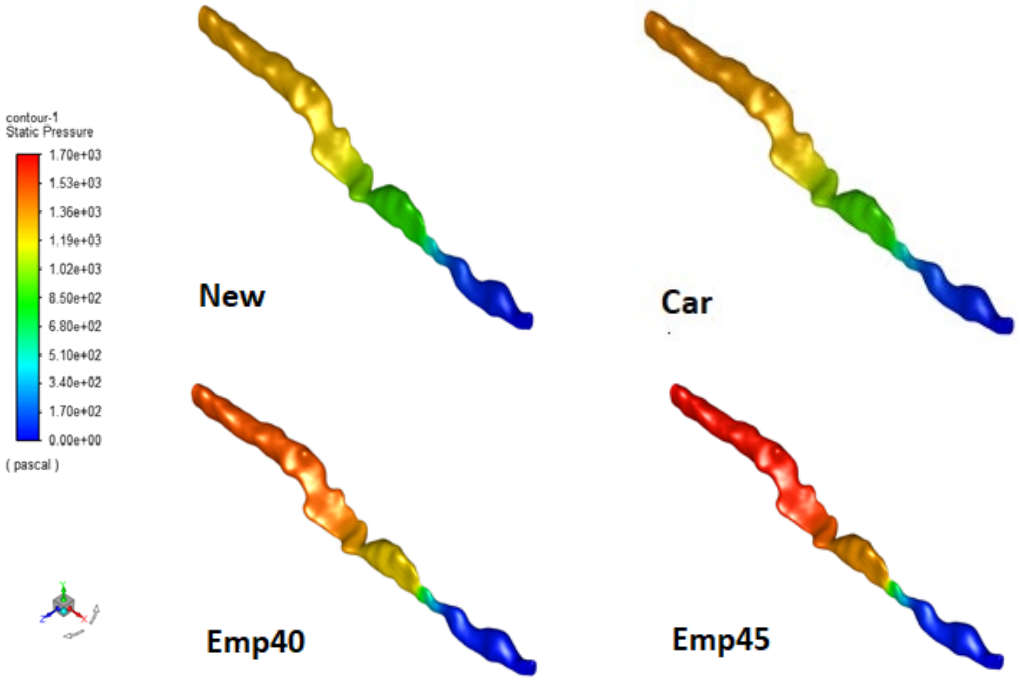

Figure 4. 3: The pressure contour along the capillary segment, (New) Newtonian model, (Car) Carreau model, (Emp40) empirical relation with H_t of 0.40 (Emp45) empirical relation with H_t of 0.45

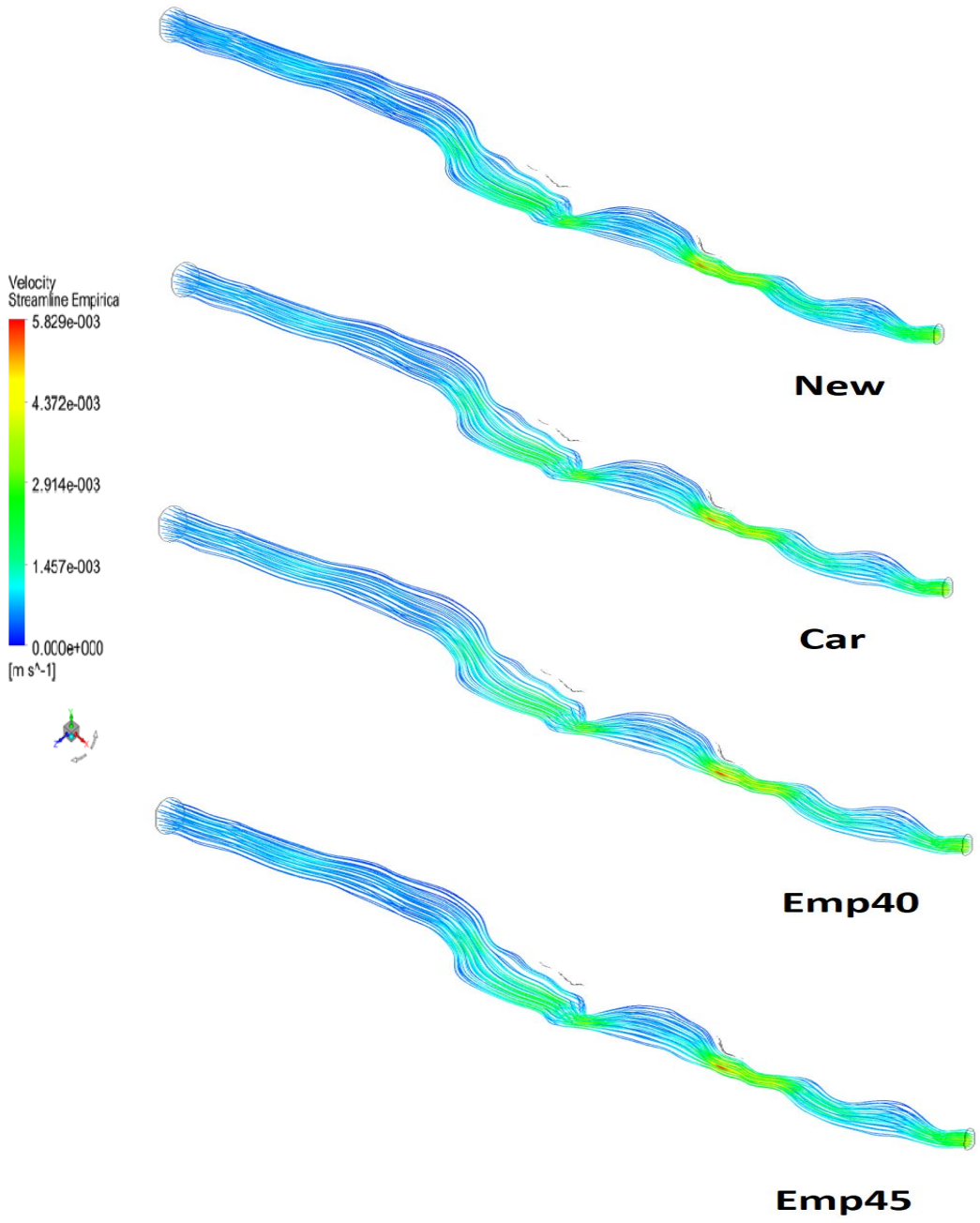

Figure 4. 4: The velocity streamlines along the capillary segment, (New) Newtonian model, (Car) Carreau model, (Emp40) empirical relation with H_t of 0.40 (Emp45) empirical relation with H_t of 0.45

In order to make the comparison between the cases more comprehensible three sections along the segments are chosen for further examination Fig 4.5. The first two sections are chosen since their cross-sectional areas and hence their viscosities are at the highest and lowest value. The last section is placed where the viscosity values of the flow experience the highest gradient.

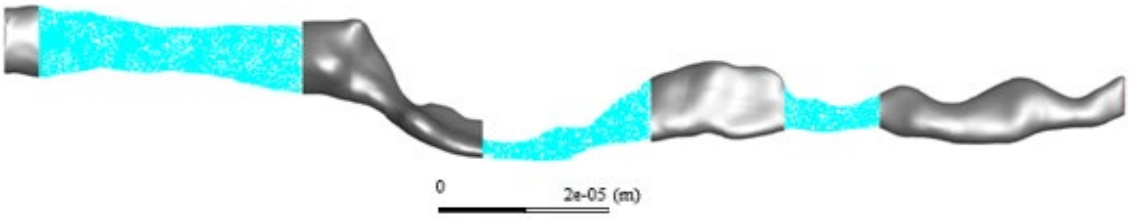

Figure 4. 5: The three sections along the segment chosen for further studies.

The first section highlighted in Fig 4.6 has the largest cross-sectional areas along the segment. The pressure, velocity, and vorticity contour of the first segment are available in Fig 4.7, 4.8, and 4.9.

Figure 4. 6: The first section along the segment chosen for further studies.

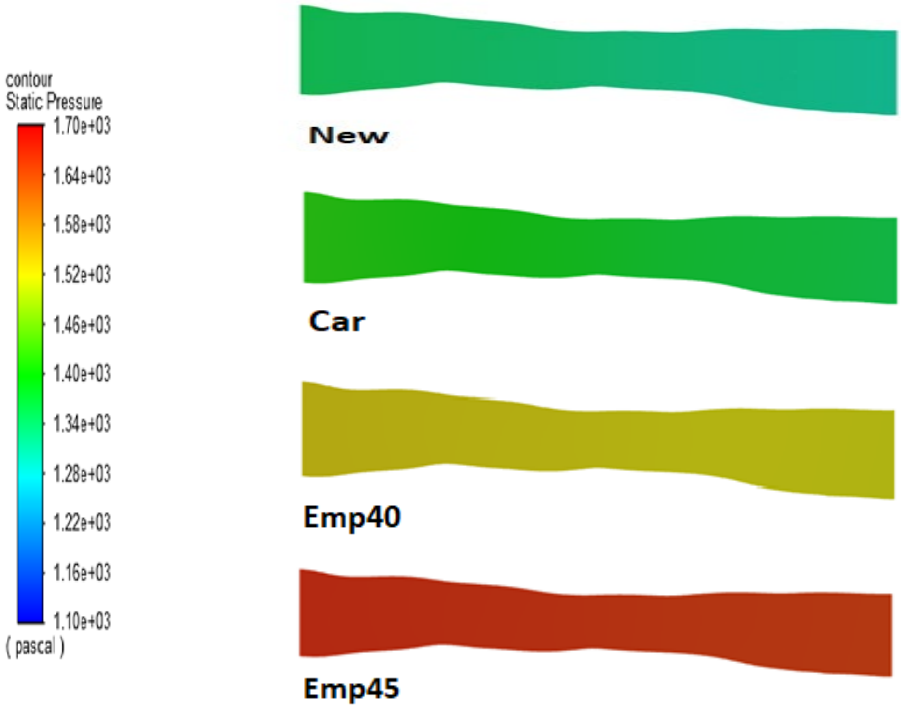

Figure 4. 7: The pressure contour of the first section along the segment, (New) Newtonian model, (Car) Carreau model, (Emp40) empirical relation with H_t of 0.40 (Emp45) empirical relation with H_t of 0.45

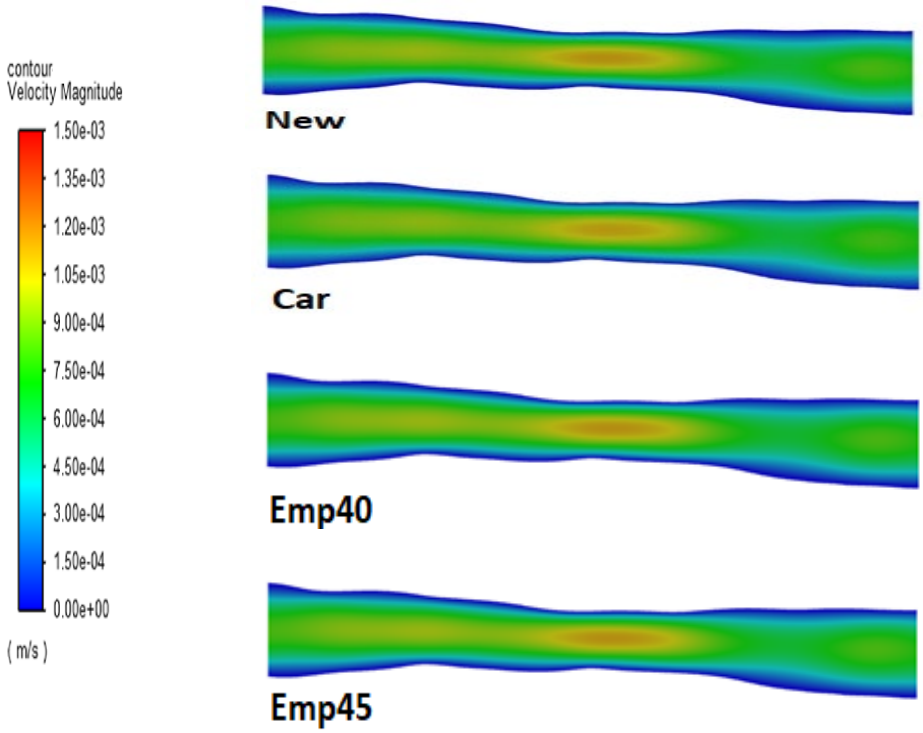

Figure 4. 8: The velocity contour of the first section along the segment, (New) Newtonian model, (Car) Carreau model, (Emp40) empirical relation with H_t of 0.40 (Emp45) empirical relation with H_t of 0.45

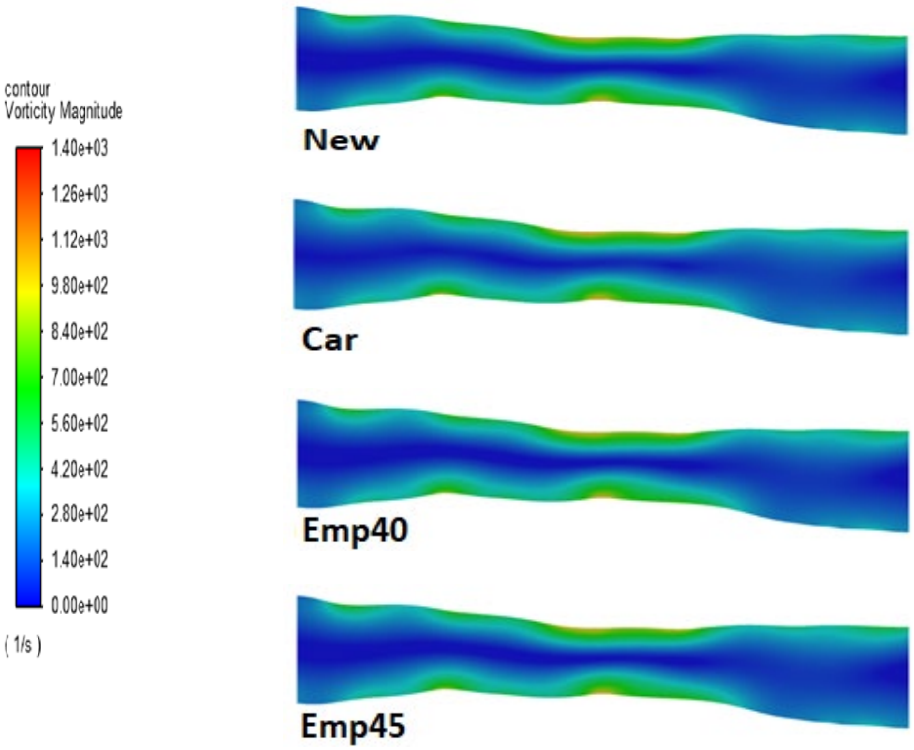

Figure 4. 9: Vorticity contour of the first section along the segment, (New) Newtonian model, (Car) Carreau model, (Emp40) empirical relation with H_t of 0.40 (Emp45) empirical relation with H_t of 0.45

The pressure contour Fig 4.7 of the first segment shows a great difference between the models. Although there is no noticeable difference in the velocity and vorticity contour, the Carreau model Fig 4.8 and Fig 4.9 exhibits the highest vorticity while showing a little bit lower velocity contour compared to the other models.

The second section highlighted in Fig 4.10 has the highest gradient of the cross-sectional area along the segment. The pressure, velocity and vorticity contour of the section are available in Fig 4.11, 4.12 and 4.13.

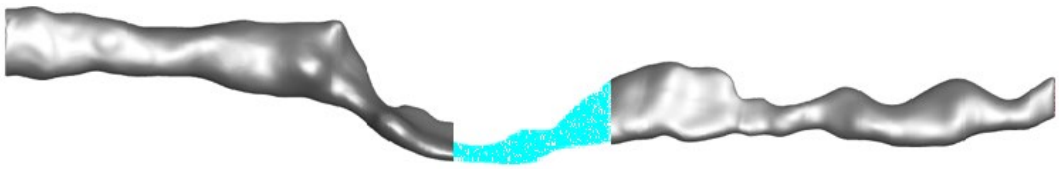

Figure 4. 10: The second section chosen for further studies.

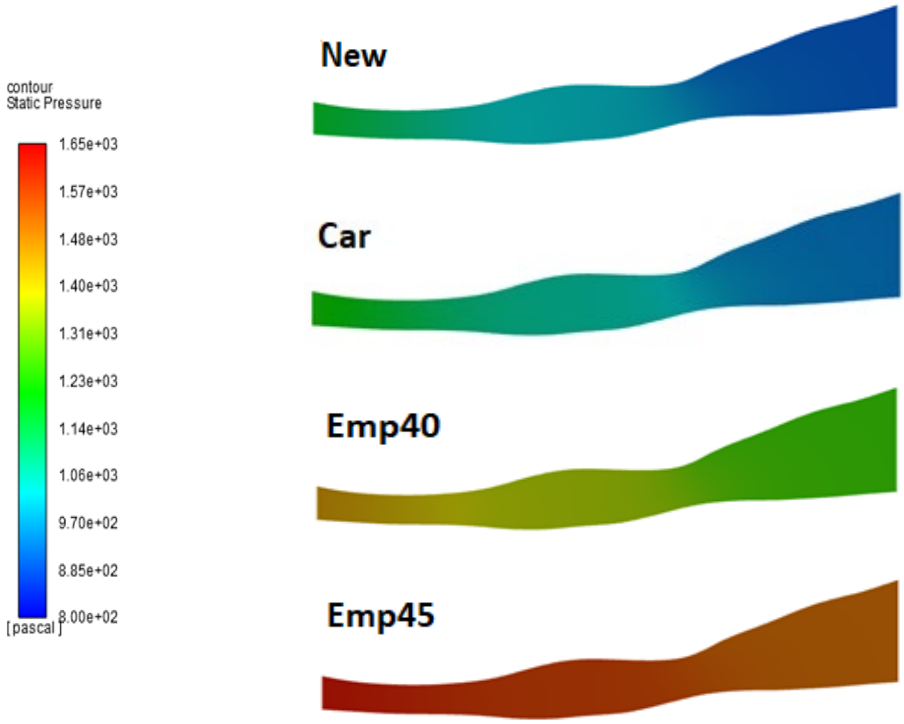

Figure 4. 11: The pressure contour of the second section along the segment, (New) Newtonian model, (Car) Carreau model, (Emp40) empirical relation with H_t of 0.40 (Emp45) empirical relation with H_t of 0.45

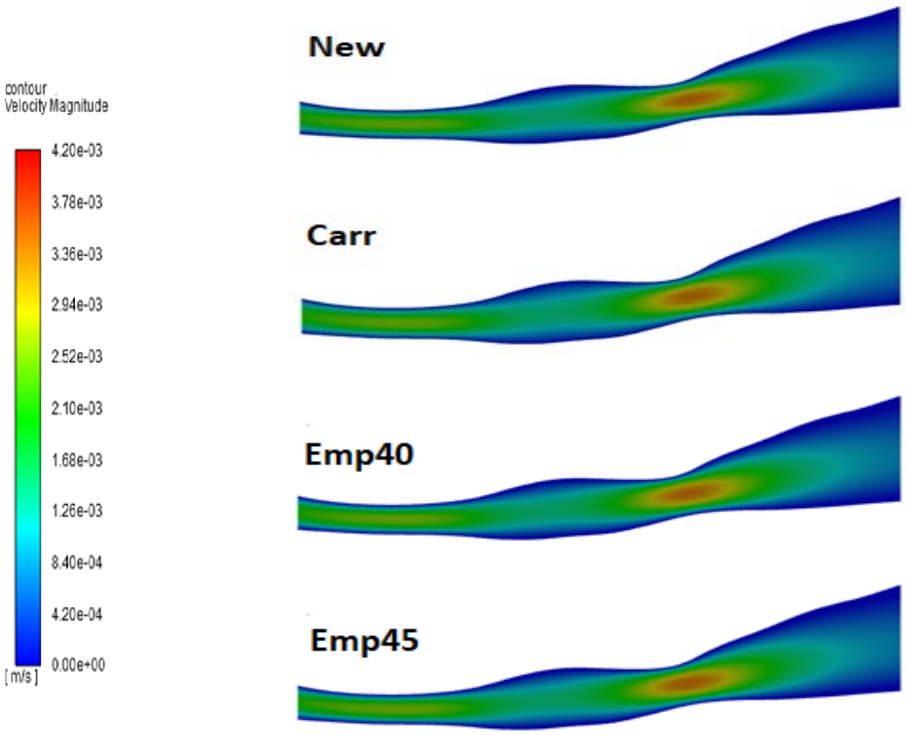

Figure 4. 12: The velocity contour of the second section along the segment, (New) Newtonian model, (Car) Carreau model, (Emp40) empirical relation with H_t of 0.40 (Emp45) empirical relation with H_t of 0.45

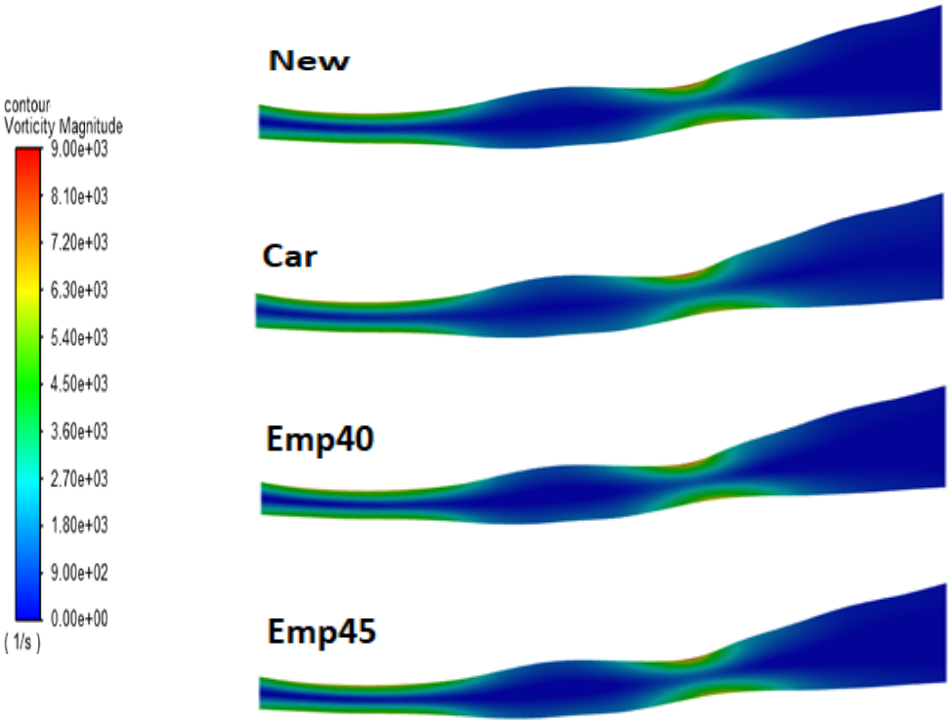

Figure 4. 13: The vorticity contour of the second section along the segment, (New) Newtonian model, (Car) Carreau model, (Emp40) empirical relation with H_t of 0.40 (Emp45) empirical relation with H_t of 0.45

The pressure contour Fig 4.11 of the second segment shows a great difference between the models with the empirical relation with H_t of 0.45 having the highest pressure. Although there is no noticeable difference in the velocity and vorticity contour, the same model Fig 4.12 and Fig 4.13 exhibits the highest velocity while showing a little bit lower vorticity contour compared to the other models.

The last section highlighted in Fig 4.14 has the smallest cross-sectional areas along the segment. The pressure, velocity and vorticity contour of the section are available in Fig 4.15, 4.16 and 4.17.

Figure 4. 14: The last section along the segment chosen for further studies.

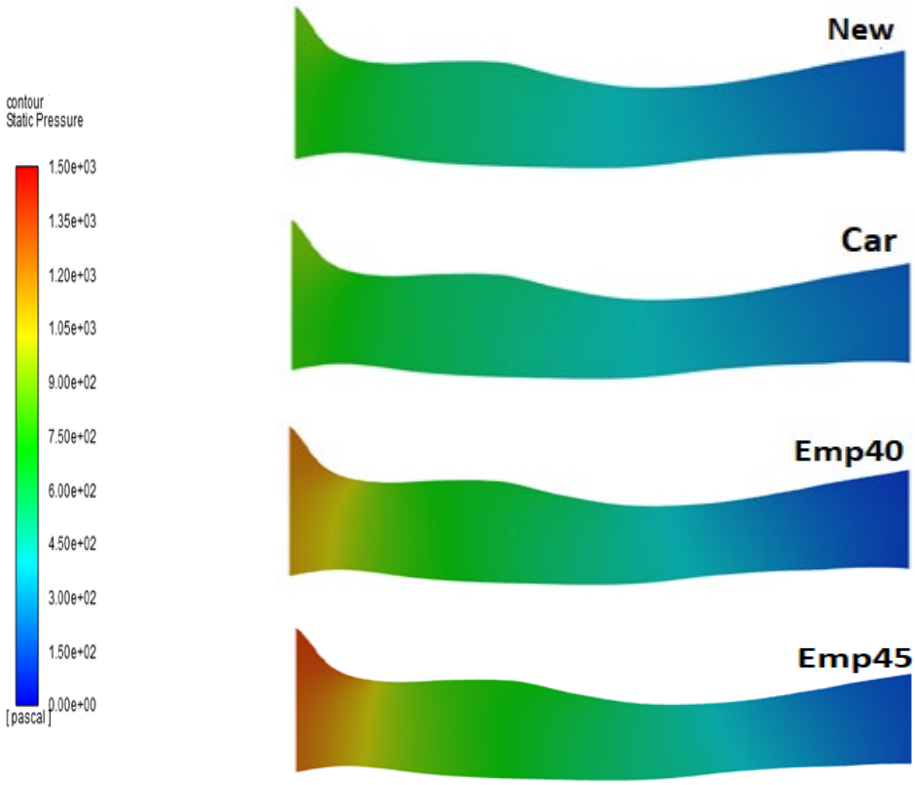

Figure 4. 15: The pressure contour of the third section along the segment, (New) Newtonian model, (Car) Carreau model, (Emp40) empirical relation with H_t of 0.40 (Emp45) empirical relation with H_t of 0.45

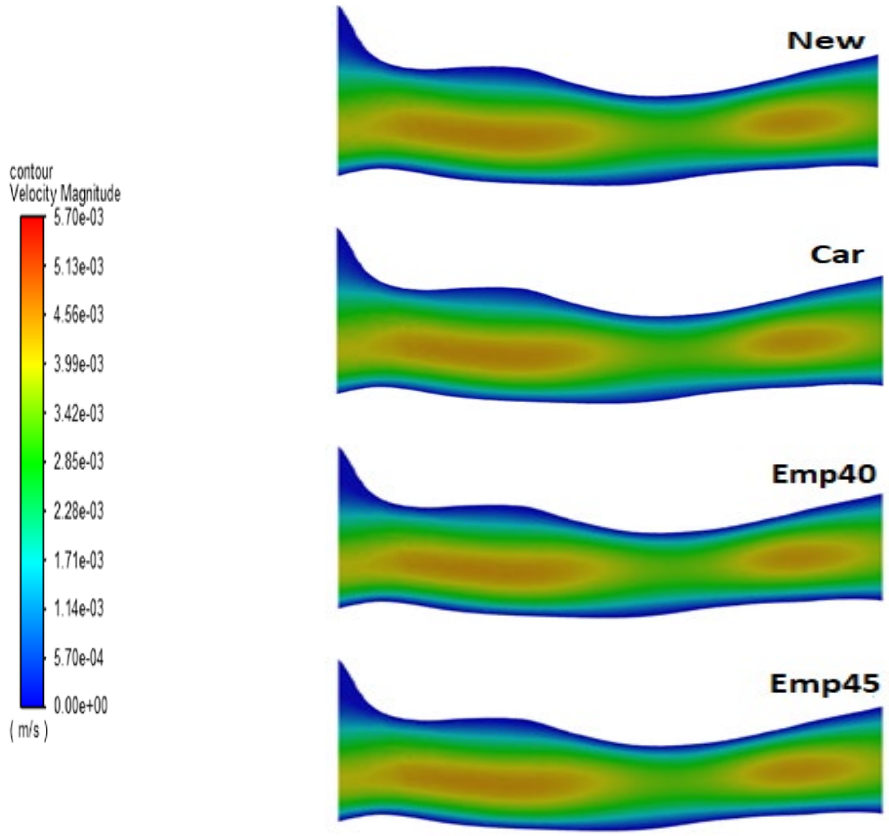

Figure 4. 16: The velocity contour of the third section along the segment, (New) Newtonian model, (Car) Carreau model, (Emp40) empirical relation with H_t of 0.40 (Emp45) empirical relation with H_t of 0.45

The pressure contour of the third segment, which has the smallest cross-sectional area, is available in Fig 4.15. It could be noted that the empirical relation with H_t of 0.45 have the highest pressure gradient while the Newtonian model faces the lowest pressure gradient. Although there is no noticeable difference in the velocity and vorticity contour, the Carreau model Fig 4.16 and Fig 4.17 exhibits the highest vorticity while showing a little bit lower velocity contour compared to the other models.

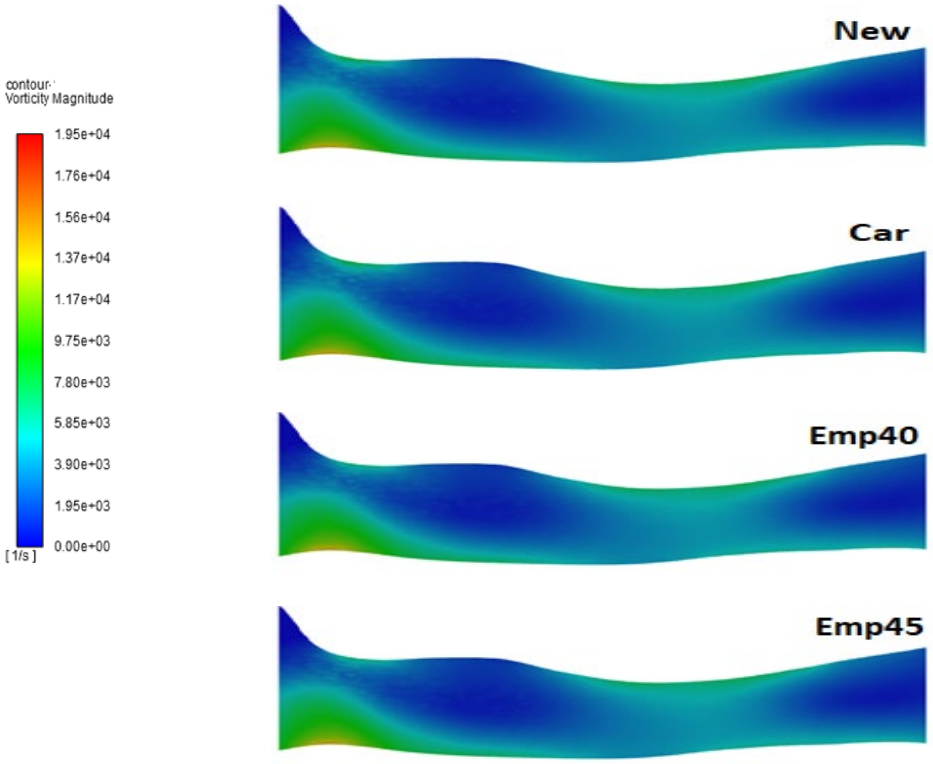

Figure 4. 17: The vorticity contour of the third section along the segment, (New) Newtonian model, (Car) Carreau model, (Emp40) empirical relation with H_t of 0.40 (Emp45) empirical relation with H_t of 0.45

For further investigation, cross-sections of the segments are put under the microscope. The cross-sections are placed at the beginning and the end of three sections previously discussed. This resulted in a total of 6 cross-sectional areas along the segment. The first and second sections have the highest viscosities, the middle sections have the highest viscosity gradient, and the last two sections have the lowest viscosities. Fig 4.18. The pressure, velocity, and vorticity contours of the various models are available in Fig 4.19, 4.20 and 4.21. Three different scale bars are available in these figures to enable a clearer view of the similarities and differences between the sections.

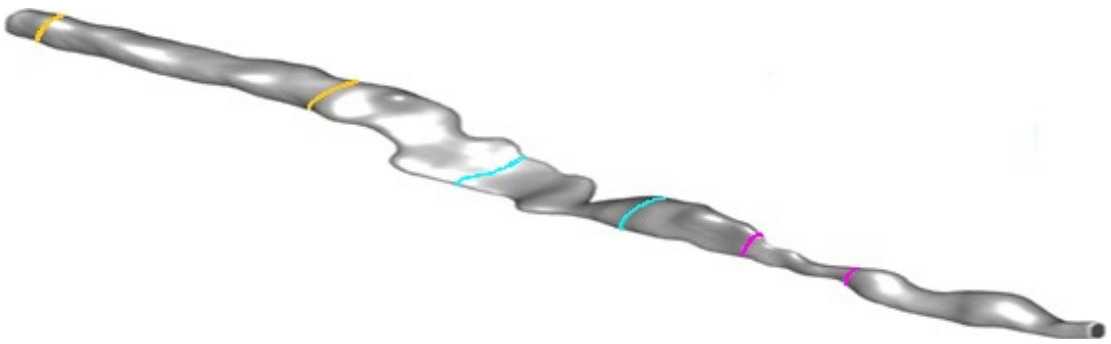

Figure 4. 18: The cross-sections chosen for further studies. The sections highlighted in orange have the highest viscosities, the sections highlighted in blue have the highest gradient in viscosity while the sections in pink have the lowest viscosities.

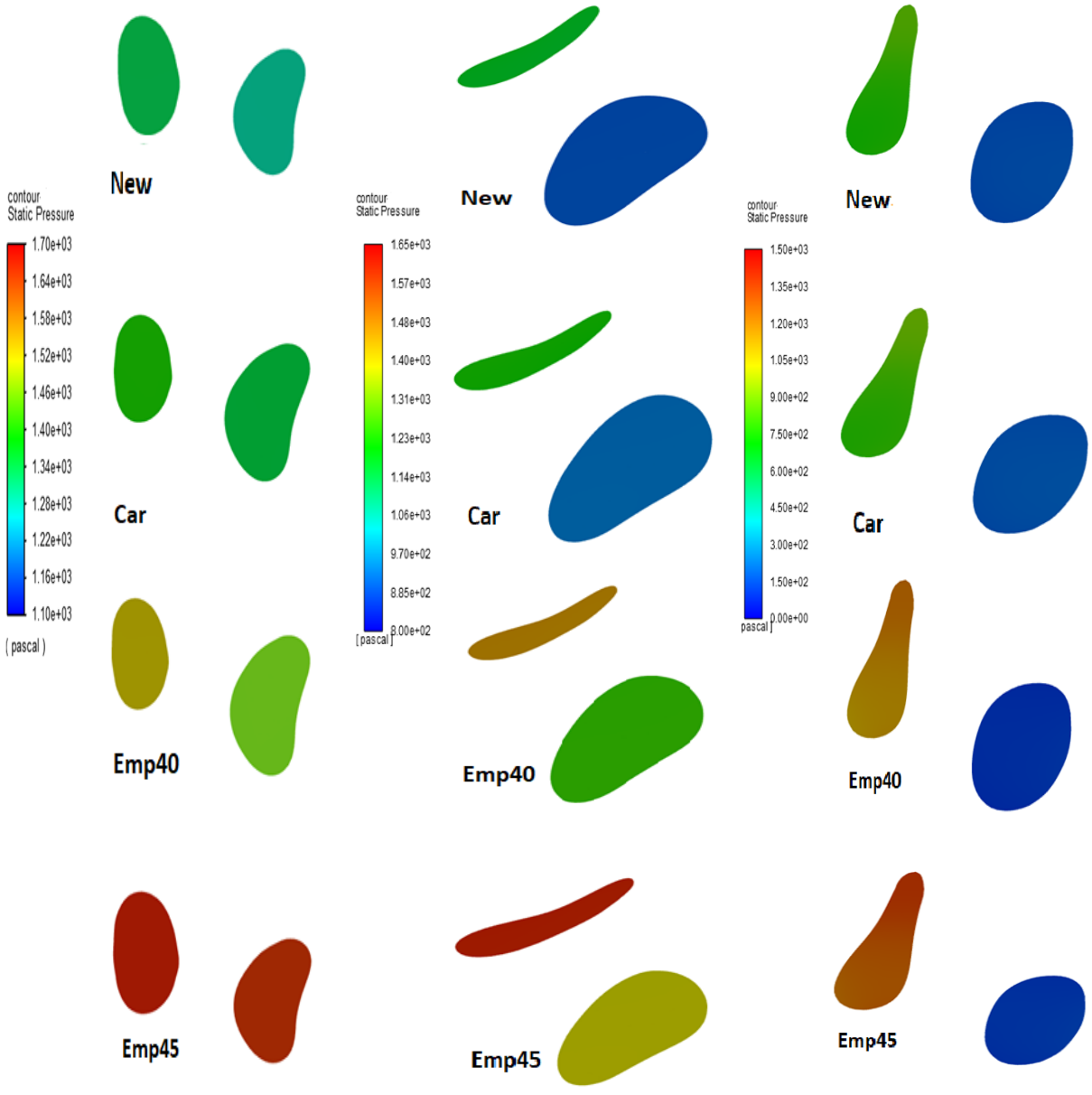

Figure 4. 19: Pressure contour of the different models at 6 different locations along the segment. The sections on the left-hand side have the highest viscosities, the sections in the middle have the highest gradient in viscosity while the sections on the right-hand side have the lowest viscosities.

The pressure contour Fig 4.19 exhibits a great difference between the models with the empirical relation with H_t of 0.45 having the highest pressure gradient while the Newtonian model faces the lowest pressure gradient. Although there is no noticeable difference in the velocity and vorticity contour Fig 4.20 and Fig 4.21, Carreau model exhibits the highest vorticity while showing a little bit lower velocity contour. Empirical relation with H_t of 0.45 exhibits the highest velocity at some locations along the segment while showing a little bit lower vorticity contour compared to the other models.

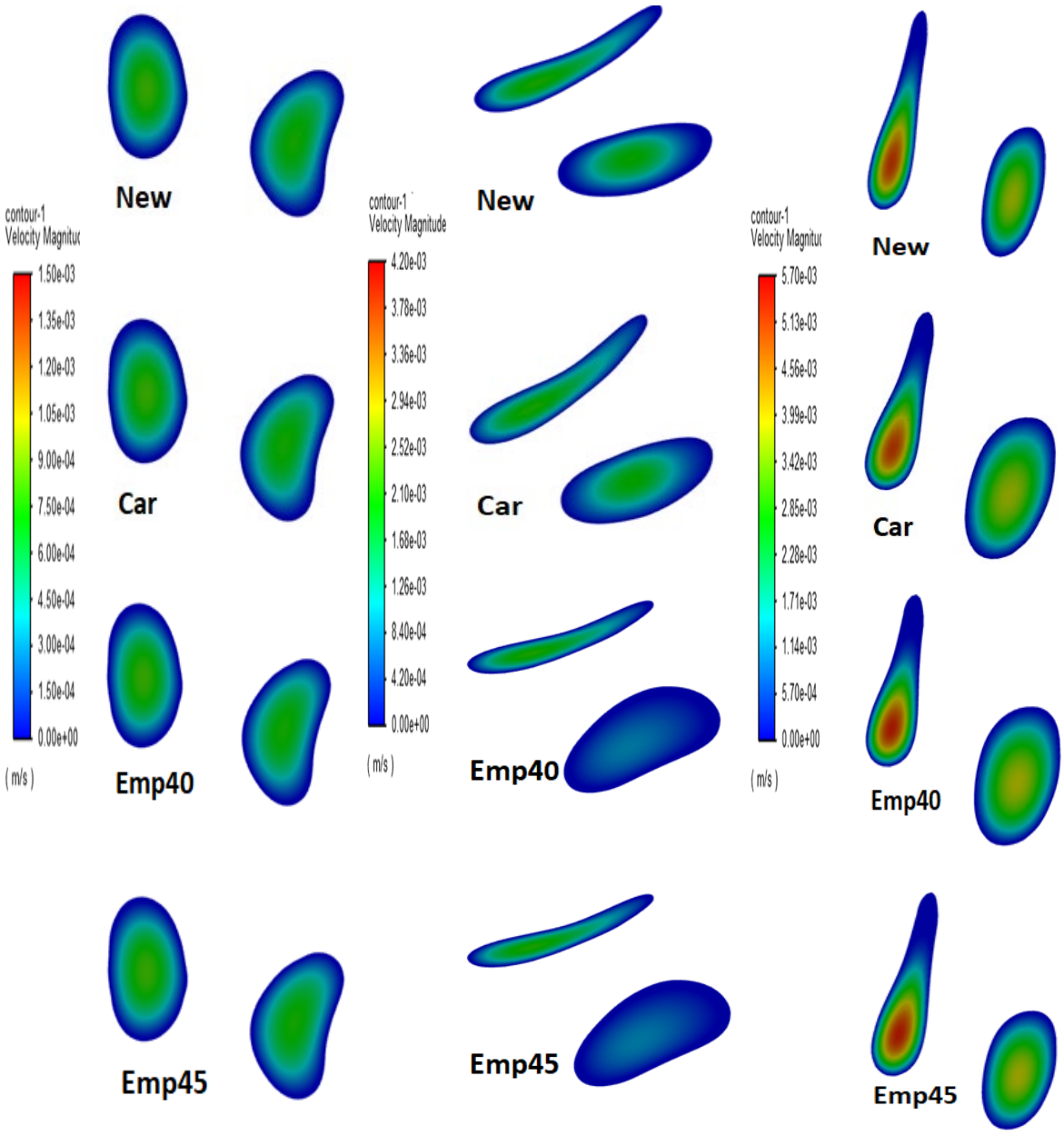

Figure 4. 20: Velocity contour of the different models at 6 different locations along the segment. The sections on the left-hand side have the highest viscosities, the sections in the middle have the highest gradient in viscosity while the sections on the right-hand side have the lowest viscosities.

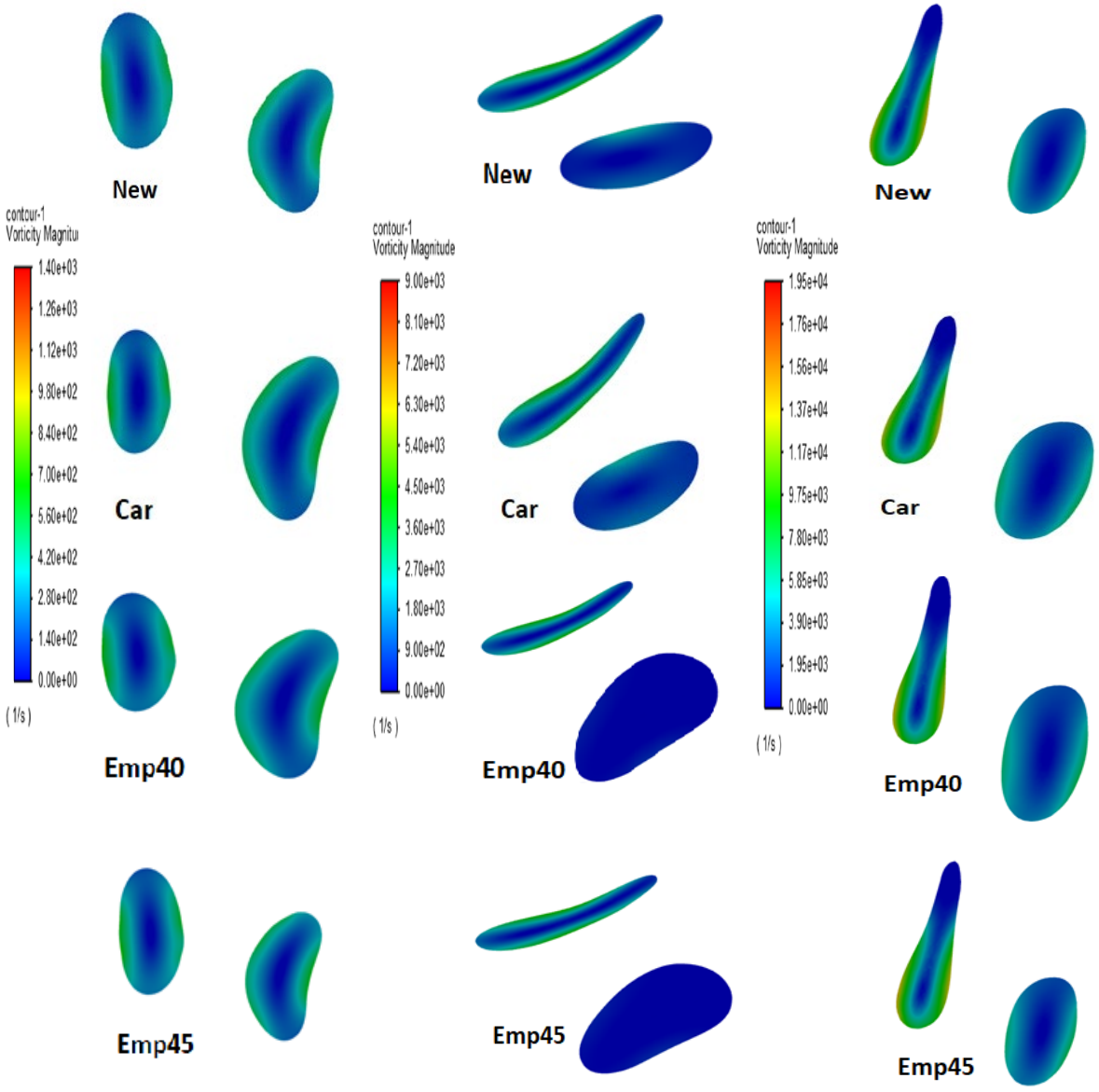

Figure 4. 21: Vorticity contour of the different models at 6 different locations along the segment. The sections on the left-hand side have the highest viscosities, the sections in the middle have the highest gradient in viscosity while the sections on the right-hand side have the lowest viscosities.

In all four cases, the pressure drop is probably the most visible difference. The Newtonian model had a pressure drop of 1417 Pa, the Carreau model had a pressure drop of 1479 Pa, the empirical model with a hematocrit of 0.40 had a pressure drop of 1556 Pa, and the last case had the largest pressure drop of 1698 Pa. It has been shown that increasing the hematocrit value from 40% to 45% leads to a noticeable increase in the pressure drop. In terms of viscosity and vorticity, there was no discernible difference between the four cases.

The Newtonian model's results were found to be similar to those of the Carreau model. However, in comparison to the Newtonian model, the Carreau model showed a greater approximation to the latter two cases.

5. CONCLUSION

Blood flow analysis has been a paramount research topic in biomechanics. Every year, numerous papers investigating blood flow are published. However, many of the published results are not comparable. Some of them even present conflicting results. Although numerical inaccuracies and experimental uncertainties may cause some inconsistency in the results, the main reason behind having conflicting results is comparing cases that are incomparable.

The number of published articles investigating blood flow increase each year, still it is difficult to compare the findings of many of these publications. This is due to the employment of various flow settings, geometry, and even different dimensions of the same geometry. It's also challenging to compare the outcomes because many of the published studies are missing information.

It is known that the dimensions of the geometry are an important factor that affects the results of the simulations. Nevertheless, having matching geometries is not enough for having comparable results; as having matching flow settings is equally important. This includes; wall elasticity, velocity profile, roughness of the wall, etc. ignoring or having non-identical values of any of these settings may influence the results. It is worth noting that the boundary conditions of the flow change along the circulatory system. Furthermore, the aforementioned flow settings differ from one human to another. While subject-specific flow settings may produce more accurate results, it also creates a unique situation with unique data that are difficult to compare.

Hitherto, there is no universally accepted computational model of the human blood flow. This is primarily owing to the complexity of the field. Even though the literature is full of studies investigating different models of blood flow, many of the models that demonstrated promising results in one study had discouraging results in others. Even if the exact flow settings were to be applied, a variation in the results may arise due to using different vessel geometry or even using the same geometry with different dimension.

In order to investigate the blood flow in capillaries a computational tool was first selected. In this study, ANSYS Fluent, a widely used industry-leading software was chosen to perform the simulations. Following that, it was necessary to determine the approach that would be used to model the blood flow in capillary. The choice of the approach depends on the complexity of the application. One-phase flow was a recommended choice that has been used in many articles. However, the difference between one-phase and multi-phase blood flow in capillaries was explored before choosing this approach.

The numerical study published by Windes et al. in 2016 [88] was taken as a reference to investigate the difference between using one-phase and multi-phase blood flow. The pressure drop results of the performed one-phase simulations were identical to the multi-phase results found by Windes et al., [88]. Thus, a single-phase flow was chosen for modeling the segments.

The three-Dimensional confocal microscopy images of a capillary segment from fixed mouse retina was processed using SpaceClaim before being used in the simulation. The use of a capillary segment visualized by high-resolution microscopic imaging of retinal tissue allowed testing the models in a more realistic environment, as capillaries are not simple tubular structures but have irregular geometries by constricting elements, like pericytes in their walls.

The segment used in this study has a unique structure with an accurate illustration of the deviations found along the segment. To the best of the author's knowledge there has not been any segment used the literature to investigate the blood flow with such an accurate representations of the structure of the micro-vessels.

In this study, three models were chosen to investigate the blood flow in the capillary segment. The first model was the Newtonian model with a constant viscosity of 0.0035 Pa.s along the segment. The second model was the Carreau model. While, the last

two simulations used the empirical relation proposed by Pries et al., [98] with hematocrit of 0.40 and 0.45 respectively.

In the previous section, the streamlines, pressure, velocity, and vorticity findings from the four simulations were compared. Moreover, three sections and 6 cross-sectional areas were chosen for further examination to make the comparison between the cases more comprehensible. The sections were chosen where the viscosities are at the highest and lowest value and where the viscosity undergoes the highest gradient in value.

In this study, the pressure drop was the foremost result which is expected due to the changing viscosity. The Newtonian model had a pressure drop of 1.42 kPa, the Carreau model had a pressure drop of 1.48 kPa, the empirical model with a hematocrit of 0.40 had a pressure drop of 1.56 kPa, and the last case had the largest pressure drop of 1.70 kPa. Changing the model has a minor impact on the results of the velocity and vorticity. This can be attributed to the trivial impact of the viscosity part in Eq. 4 which is used in the FLUENT solver. The viscosity part in momentum equation has a small effect due to being the product of the small value acceleration.

It has been noticed that increasing the hematocrit value, even by a small percentage, leads to a noticeable increase in the pressure drop. The change of the inlet velocity, even by a small percentage, also has a huge impact on the pressure drop. In terms of viscosity and vorticity, there was no discernible difference between the four cases.

The results of the Newtonian model were found to be close to those of the Carreau model. In comparison to the Newtonian model, the Carreau model showed a better approximation to the last two cases. Nonetheless, since the last model is highly dependent on the cross-sectional area of the geometry, any change in the dimensions will have a significant impact on the results. In fact, an increase in the average cross sectional area by 2-3 μm will result in having a pressure drop even lower than that of the Newtonian model.

While velocity and vorticity profiles were virtually identical in all models, the striking difference in pressure profile is interesting and must be carefully interpreted. Pressure gradient across a capillary segment is the main driving force that determines the plasma and cell velocity. However, in all tissues, capillaries form dense interconnected networks and a pressure change in any segment will be immediately transmitted to the upstream and downstream capillaries, affecting the overall blood flow in the network.

This work shows that the choice of an appropriate model, that will accurately represents the blood elements in capillaries, is crucial for computations. The cross-sectional area changes due to contractile actions of the capillary wall. For example, pericytes or luminal narrowing by endothelial or astrocyte endfeet swelling which can significantly affect the pressure distribution. This can be simulated by the utilization of an appropriate rheological model. The red blood cell fraction also seems to be a determinant of the pressure gradients across luminal irregularities, as previously revealed by the effect of hematocrit ratio.

6. REFERENCES

[1] M. Lovett, K. Lee, A. Edwards, and D. L. Kaplan, “Vascularization strategies for tissue engineering.,” *Tissue Eng. Part B. Rev.*, vol. 15, no. 3, pp. 353–70, Sep. 2009, doi: 10.1089/ten.TEB.2009.0085.

[2] C. M. Jones *et al.*, “Measurement science in the circulatory system.,” *Cell. Mol. Bioeng.*, vol. 7, no. 1, pp. 1–14, Mar. 2014, doi: 10.1007/s12195-013-0317-4.

[3] R. N. Pittman, *Regulation of Tissue Oxygenation*, vol. 3, no. 3. 2011.

[4] P. J. Wallace, N. T. Connell, and J. L. Abkowitz, “Blood Forum The role of hematologists in a changing United States health care system,” vol. 125, no. 16, pp. 2467–2471, 2016, doi: 10.1182/blood-2014-12-615047.The.

[5] D. Hay, C. S. R. Hatton, and D. J. Weatherall, “The future of academic haematology,” *Br. J. Haematol.*, vol. 176, no. 5, pp. 721–727, Mar. 2017, doi: 10.1111/bjh.14472.

[6] R. F. Padmore *et al.*, “Importance of the hematology laboratory in infectious disease diagnosis by morphology: Four educational case studies.,” *Int. J. Lab. Hematol.*, vol. 42 Suppl 1, pp. 133–137, 2020, doi: 10.1111/ijlh.13227.

[7] J. L. Frater, G. Zini, G. D’Onofrio, and H. J. Rogers, “COVID-19 and the clinical hematology laboratory,” *Int. J. Lab. Hematol.*, vol. 42, no. S1, pp. 11–18, Jun. 2020, doi: 10.1111/ijlh.13229.

[8] A. M. Robertson, A. Sequeira, and R. G. Owens, “Rheological models for blood,” in *Cardiovascular Mathematics*, Milano: Springer Milan, 2009, pp. 211–241.

[9] D. J. Castillo, R. F. Rifkin, D. A. Cowan, and M. Potgieter, “The Healthy Human Blood Microbiome: Fact or Fiction?,” *Front. Cell. Infect. Microbiol.*, vol. 9, May 2019, doi: 10.3389/fcimb.2019.00148.

[10] Blood Pressure Lowering Treatment Trialists’ Collaboration *et al.*, “Effects of different regimens to lower blood pressure on major cardiovascular events in older and younger adults: meta-analysis of randomised trials.,” *BMJ*, vol. 336, no. 7653, pp. 1121–3, May 2008, doi: 10.1136/bmj.39548.738368.BE.

[11] R. Hajar, “The pulse in ancient medicine part 1,” *Hear. Views*, vol. 19, no. 1, p. 36,

2018, doi: 10.4103/HEARTVIEWS.HEARTVIEWS_23_18.

[12] A. N. Al-Shura, “Hematology,” in *Integrative Cardiovascular Chinese Medicine*, Elsevier, 2014, pp. 81–93.

[13] L. Waite, *Biofluid mechanics in cardiovascular systems*. New York: McGraw-Hill, 2006.

[14] K. Tanishita and K. Yamamoto, Eds., *Vascular Engineering*. Tokyo: Springer Japan, 2016.

[15] S. K. Ramasamy, “Structure and Functions of Blood Vessels and Vascular Niches in Bone,” *Stem Cells Int.*, vol. 2017, pp. 1–10, 2017, doi: 10.1155/2017/5046953.

[16] R. Chaudhry, J. H. Miao, and A. Rehman, *Physiology, Cardiovascular*. 2020.

[17] Y. Itoh and N. Suzuki, “Control of brain capillary blood flow.,” *J. Cereb. Blood Flow Metab.*, vol. 32, no. 7, pp. 1167–76, Jul. 2012, doi: 10.1038/jcbfm.2012.5.

[18] R. Daneman and A. Prat, “The blood-brain barrier.,” *Cold Spring Harb. Perspect. Biol.*, vol. 7, no. 1, p. a020412, Jan. 2015, doi: 10.1101/cshperspect.a020412.

[19] G. Bergers and S. Song, “The role of pericytes in blood-vessel formation and maintenance.,” *Neuro. Oncol.*, vol. 7, no. 4, pp. 452–64, Oct. 2005, doi: 10.1215/S1152851705000232.

[20] Y. Ando *et al.*, “Brain-Specific Ultrastructure of Capillary Endothelial Glycocalyx and Its Possible Contribution for Blood Brain Barrier.,” *Sci. Rep.*, vol. 8, no. 1, p. 17523, 2018, doi: 10.1038/s41598-018-35976-2.

[21] A. R. Pries, T. W. Secomb, H. Jacobs, M. Sperandio, K. Osterloh, and P. Gaehtgens, “Microvascular blood flow resistance: role of endothelial surface layer.,” *Am. J. Physiol.*, vol. 273, no. 5, pp. H2272-9, 1997, doi: 10.1152/ajpheart.1997.273.5.H2272.

[22] T. W. Secomb, R. Hsu, and A. R. Pries, “Motion of red blood cells in a capillary with an endothelial surface layer: effect of flow velocity,” *Am. J. Physiol. Circ. Physiol.*, vol. 281, no. 2, pp. H629–H636, Aug. 2001, doi: 10.1152/ajpheart.2001.281.2.H629.

[23] E. Witzleb, “Functions of the Vascular System,” in *Human Physiology*, Berlin, Heidelberg: Springer Berlin Heidelberg, 1989, pp. 480–542.

[24] I. G. Gould, P. Tsai, D. Kleinfeld, and A. Linninger, “The capillary bed offers the largest hemodynamic resistance to the cortical blood supply.,” *J. Cereb. Blood Flow Metab.*, vol. 37, no. 1, pp. 52–68, 2017, doi: 10.1177/0271678X16671146.

[25] C. D. Murray, “The Physiological Principle of Minimum Work: I. The Vascular System and the Cost of Blood Volume,” *Proc. Natl. Acad. Sci.*, vol. 12, no. 3, pp. 207–214, Mar. 1926, doi: 10.1073/pnas.12.3.207.

[26] L. Learning, “Anatomy and Physiology II,” 2020. https://courses.lumenlearning.com/ap2/.

[27] Y. C. Fung, *Biomechanics: Circulation*. New York, NY: Springer New York, 1996.

[28] Y. H. Kim, P. J. VandeVord, and J. S. Lee, “Multiphase non-Newtonian effects on pulsatile hemodynamics in a coronary artery,” *Int. J. Numer. Methods Fluids*, vol. 58, no. 7, pp. 803–825, Nov. 2008, doi: 10.1002/fld.1768.

[29] Y. A. Cengel and J. M. Cimbala, *Fluid mechanics: Fundamentals and applications*, 3rd ed. Columbus, OH: McGraw-Hill Education, 2017.

[30] E. Nader *et al.*, “Blood Rheology: Key Parameters, Impact on Blood Flow, Role in Sickle Cell Disease and Effects of Exercise,” *Front. Physiol.*, vol. 10, Oct. 2019, doi: 10.3389/fphys.2019.01329.

[31] P. Connes, T. Alexy, J. Detterich, M. Romana, M.-D. Hardy-Dessources, and S. K. Ballas, “The role of blood rheology in sickle cell disease.,” *Blood Rev.*, vol. 30, no. 2, pp. 111–8, Mar. 2016, doi: 10.1016/j.blre.2015.08.005.

[32] M. Nichelatti, P. Pettazzoni, and G. Pallotti, “The study of viscoelastic behavior of blood vessels,” *Blood, Hear. Circ.*, vol. 1, no. 2, 2017, doi: 10.15761/BHC.1000110.

[33] P. Eslami *et al.*, “Effect of Wall Elasticity on Hemodynamics and Wall Shear Stress in Patient-Specific Simulations in the Coronary Arteries.,” *J. Biomech. Eng.*, vol. 142, no. 2, 2020, doi: 10.1115/1.4043722.

[34] J. Vent-Schmidt *et al.*, “Blood Thixotropy in Patients with Sickle Cell Anaemia: Role of Haematocrit and Red Blood Cell Rheological Properties,” *PLoS One*, vol. 9, no. 12, p. e114412, Dec. 2014, doi: 10.1371/journal.pone.0114412.

[35] T.-W. Lee, K.-S. Bae, H. S. Choi, and M.-J. Chern, “Computational Simulations

of Flow and Oxygen/Drug Delivery in a Three-Dimensional Capillary Network," *ISRN Biomath.*, vol. 2014, pp. 1–11, Apr. 2014, doi: 10.1155/2014/359327.

[36] S. A. Reid *et al.*, "Study of hematological and biochemical parameters in runners completing a standard marathon.," *Clin. J. Sport Med.*, vol. 14, no. 6, pp. 344–53, Nov. 2004, doi: 10.1097/00042752-200411000-00004.

[37] K. S. Saladin, *Anatomy & Physiology: The Unity of Form and Function*. McGraw-Hill Higher Education, 2003.

[38] J. G. Betts *et al.*, *Anatomy and Physiology*. Houston, Texas: OpenStax College, Rice University, 2013.

[39] N. D. Botkin, A. E. Kovtanyuk, V. L. Turova, I. N. Sidorenko, and R. Lampe, "Accounting for Tube Hematocrit in Modeling of Blood Flow in Cerebral Capillary Networks.," *Comput. Math. Methods Med.*, vol. 2019, p. 4235937, 2019, doi: 10.1155/2019/4235937.

[40] T. Sochi, "Non-Newtonian Rheology in Blood Circulation," *arXiv:1306.2067*, 2013.

[41] D. S. Sankar and K. Hemalatha, "A non-Newtonian fluid flow model for blood flow through a catheterized artery—Steady flow," *Appl. Math. Model.*, vol. 31, no. 9, pp. 1847–1864, Sep. 2007, doi: 10.1016/j.apm.2006.06.009.

[42] H. Noguchi and G. Gompper, "Shape transitions of fluid vesicles and red blood cells in capillary flows," *Proc. Natl. Acad. Sci.*, vol. 102, no. 40, pp. 14159–14164, Oct. 2005, doi: 10.1073/pnas.0504243102.

[43] J. H. Jeong, Y. Sugii, M. Minamiyama, and K. Okamoto, "Measurement of RBC deformation and velocity in capillaries in vivo.," *Microvasc. Res.*, vol. 71, no. 3, pp. 212–7, May 2006, doi: 10.1016/j.mvr.2006.02.006.

[44] R. Huisjes, A. Bogdanova, W. W. van Solinge, R. M. Schiffelers, L. Kaestner, and R. van Wijk, "Squeezing for Life - Properties of Red Blood Cell Deformability.," *Front. Physiol.*, vol. 9, p. 656, 2018, doi: 10.3389/fphys.2018.00656.

[45] R. Skalak and P. I. Branemark, "Deformation of red blood cells in capillaries.," *Science*, vol. 164, no. 3880, pp. 717–9, May 1969, doi: 10.1126/science.164.3880.717.

[46] S. Chien, "Red cell deformability and its relevance to blood flow.," *Annu. Rev.*

Physiol., vol. 49, pp. 177–92, 1987, doi: 10.1146/annurev.ph.49.030187.001141.

[47] J. G. Danielczok *et al.*, "Red Blood Cell Passage of Small Capillaries Is Associated with Transient Ca2+-mediated Adaptations.," *Front. Physiol.*, vol. 8, p. 979, 2017, doi: 10.3389/fphys.2017.00979.

[48] N. Takeishi and Y. Imai, "Capture of microparticles by bolus flow of red blood cells in capillaries," *Sci. Rep.*, vol. 7, no. 1, p. 5381, Dec. 2017, doi: 10.1038/s41598-017-05924-7.

[49] G. W. Schmid-Schönbein, S. Usami, R. Skalak, and S. Chien, "The interaction of leukocytes and erythrocytes in capillary and postcapillary vessels.," *Microvasc. Res.*, vol. 19, no. 1, pp. 45–70, Jan. 1980, doi: 10.1016/0026-2862(80)90083-7.

[50] P. S. Ayyaswamy, "Introduction to Biofluid Mechanics," in *Fluid Mechanics*, Elsevier, 2016, pp. e1–e73.

[51] O. K. Baskurt and H. J. Meiselman, "RBC aggregation: more important than RBC adhesion to endothelial cells as a determinant of in vivo blood flow in health and disease.," *Microcirc. (New York, N.Y.)*, vol. 15, no. 7, pp. 585–90, Oct. 2008, doi: 10.1080/10739680802107447.

[52] D. J. Beebe, G. A. Mensing, and G. M. Walker, "Physics and applications of microfluidics in biology.," *Annu. Rev. Biomed. Eng.*, vol. 4, pp. 261–86, 2002, doi: 10.1146/annurev.bioeng.4.112601.125916.

[53] N.-T. Nguyen, S. T. Wereley, and S. A. M. Shaegh, *Fundamentals and Applications of Microfluidics*, 3rd ed. Artech House;, 2019.

[54] G. M. Whitesides, "The origins and the future of microfluidics," *Nature*, vol. 442, no. 7101, pp. 368–373, Jul. 2006, doi: 10.1038/nature05058.

[55] N. Convery and N. Gadegaard, "30 years of microfluidics," *Micro Nano Eng.*, vol. 2, pp. 76–91, Mar. 2019, doi: 10.1016/j.mne.2019.01.003.

[56] F. S. Collins, M. Morgan, and A. Patrinos, "The Human Genome Project: lessons from large-scale biology.," *Science*, vol. 300, no. 5617, pp. 286–90, Apr. 2003, doi: 10.1126/science.1084564.

[57] E. Choban, "Microfluidic fuel cell based on laminar flow," *J. Power Sources*, vol. 128, no. 1, pp. 54–60, Mar. 2004, doi: 10.1016/j.jpowsour.2003.11.052.

[58] B. E. Rapp, “Fluids,” in *Microfluidics: Modelling, Mechanics and Mathematics*, Elsevier, 2017, pp. 243–263.

[59] M. Ashoor, A. Khorshidi, A. Pirouzi, A. Abdollahi, M. Mohsenzadeh, and S. M. Z. Barzi, “Estimation of Reynolds number on microvasculature capillary bed using diffusion and perfusion MRI: the theoretical and experimental investigations,” *Eur. Phys. J. Plus*, vol. 136, no. 2, p. 152, Feb. 2021, doi: 10.1140/epjp/s13360-021-01145-0.

[60] D. Matienzo and B. Bordoni, *Anatomy, Blood Flow*. 2021.

[61] O. K. Baskurt and H. J. Meiselman, “Blood rheology and hemodynamics.,” *Semin. Thromb. Hemost.*, vol. 29, no. 5, pp. 435–50, Oct. 2003, doi: 10.1055/s-2003-44551.

[62] T. YAMAGUCHI, T. ISHIKAWA, K. TSUBOTA, Y. IMAI, M. NAKAMURA, and T. FUKUI, “Computational Blood Flow Analysis -New Trends and Methods,” *J. Biomech. Sci. Eng.*, vol. 1, no. 1, pp. 29–50, 2006, doi: 10.1299/jbse.1.29.

[63] J. C. Weddell, J. Kwack, P. I. Imoukhuede, and A. Masud, “Hemodynamic analysis in an idealized artery tree: differences in wall shear stress between Newtonian and non-Newtonian blood models.,” *PLoS One*, vol. 10, no. 4, p. e0124575, 2015, doi: 10.1371/journal.pone.0124575.

[64] Y. Bai and Q. Bai, “Hydraulics,” in *Subsea Engineering Handbook*, Elsevier, 2019, pp. 315–361.

[65] T. W. Secomb and A. R. Pries, “Blood viscosity in microvessels: experiment and theory.,” *Comptes rendus. Phys.*, vol. 14, no. 6, pp. 470–478, Jun. 2013, doi: 10.1016/j.crhy.2013.04.002.

[66] N. Bessonov, A. Sequeira, S. Simakov, Y. Vassilevskii, and V. Volpert, “Methods of Blood Flow Modelling,” *Math. Model. Nat. Phenom.*, vol. 11, no. 1, pp. 1–25, Dec. 2016, doi: 10.1051/mmnp/201611101.

[67] T. Chen *et al.*, “Comparison between Single-Phase Flow Simulation and Multiphase Flow Simulation of Patient-Specific Total Cavopulmonary Connection Structures Assisted by a Rotationally Symmetric Blood Pump,” *Symmetry (Basel).*, vol. 13, no. 5, p. 912, May 2021, doi: 10.3390/sym13050912.

[68] D. A. Fedosov, B. Caswell, A. S. Popel, and G. E. Karniadakis, “Blood flow and

cell-free layer in microvessels.," *Microcirculation*, vol. 17, no. 8, pp. 615–28, Nov. 2010, doi: 10.1111/j.1549-8719.2010.00056.x.

[69] V. Cristini and G. S. Kassab, "Computer Modeling of Red Blood Cell Rheology in the Microcirculation: A Brief Overview," *Ann. Biomed. Eng.*, vol. 33, no. 12, pp. 1724–1727, Dec. 2005, doi: 10.1007/s10439-005-8776-y.

[70] A. S. Popel and P. C. Johnson, "Microcirculation and Hemorheology.," *Annu. Rev. Fluid Mech.*, vol. 37, pp. 43–69, Jan. 2005, doi: 10.1146/annurev.fluid.37.042604.133933.

[71] M. O. Bernabeu *et al.*, "Impact of blood rheology on wall shear stress in a model of the middle cerebral artery.," *Interface Focus*, vol. 3, no. 2, p. 20120094, Apr. 2013, doi: 10.1098/rsfs.2012.0094.

[72] J. Jung and A. Hassanein, "Three-phase CFD analytical modeling of blood flow.," *Med. Eng. Phys.*, vol. 30, no. 1, pp. 91–103, Jan. 2008, doi: 10.1016/j.medengphy.2006.12.004.

[73] G. N. Coleman and R. D. Sandberg, "A Primer on Direct Numerical Simulation of Turbulence Methods, Procedures and Guidelines," UK, 2010.

[74] P. Balogh and P. Bagchi, "Direct Numerical Simulation of Cellular-Scale Blood Flow in 3D Microvascular Networks.," *Biophys. J.*, vol. 113, no. 12, pp. 2815–2826, Dec. 2017, doi: 10.1016/j.bpj.2017.10.020.

[75] G. Tryggvason, S. Thomas, J. Lu, and B. Aboulhasanzadeh, "Multiscale issues in DNS of multiphase flows," *Acta Math. Sci.*, vol. 30, no. 2, pp. 551–562, Mar. 2010, doi: 10.1016/S0252-9602(10)60062-8.

[76] E. Dick, "Introduction to Finite Element Methods in Computational Fluid Dynamics," in *Computational Fluid Dynamics*, Berlin, Heidelberg: Springer Berlin Heidelberg, 2009.

[77] K. S. Surana, S. Allu, P. W. Tenpas, and J. N. Reddy, "k-version of finite element method in gas dynamics: higher-order global differentiability numerical solutions," *Int. J. Numer. Methods Eng.*, vol. 69, no. 6, pp. 1109–1157, Feb. 2007, doi: 10.1002/nme.1801.

[78] C. A. Taylor, T. J. R. Hughes, and C. K. Zarins, "Finite element modeling of blood flow in arteries," *Comput. Methods Appl. Mech. Eng.*, vol. 158, no. 1–2, pp. 155–

196, May 1998, doi: 10.1016/S0045-7825(98)80008-X.

[79] I. E. Vignon-Clementel, C. Alberto Figueroa, K. E. Jansen, and C. A. Taylor, "Outflow boundary conditions for three-dimensional finite element modeling of blood flow and pressure in arteries," *Comput. Methods Appl. Mech. Eng.*, vol. 195, no. 29–32, pp. 3776–3796, Jun. 2006, doi: 10.1016/j.cma.2005.04.014.

[80] S. Appanaboyina *et al.*, "Computational modelling of blood flow in side arterial branches after stenting of cerebral aneurysms," *Int. J. Comut. Fluid Dyn.*, vol. 22, no. 10, pp. 669–676, Dec. 2008, doi: 10.1080/10618560802495255.

[81] T. M. Mubita, L. R. Rojas-Solórzano, and J. B. Moreno, "A Multiphase Approach to Model Blood Flow in Micro-tubes," 2014, pp. 235–247.

[82] "AUTODESK KNOWLEDGE NETWORK." https://knowledge.autodesk.com/support/cfd/learn-explore/caas/CloudHelp/cloudhelp/2014/ENU/SimCFD/files/GUID-12A9AED8-2047-4D3A-BC80-82BE9CF47517-htm.html (accessed Dec. 09, 2019).

[83] S. Patankar, *Numerical Heat Transfer and Fluid Flow*. CRC Press, 1980.

[84] S. S. Shibeshi and W. E. Collins, "The Rheology of Blood Flow in a Branched Arterial System.," *Appl. Rheol.*, vol. 15, no. 6, pp. 398–405, 2005, doi: 10.1901/jaba.2005.15-398.

[85] Fluent, "No Title," *12.0 ANSYS, Inc*, 2009. https://www.afs.enea.it/project/neptunius/docs/fluent/html/th/node11.htm.

[86] S. Sun and T. Zhang, "Introduction," *Reserv. Simulations*, pp. 1–22, Jan. 2020, doi: 10.1016/B978-0-12-820957-8.00001-0.

[87] S. L. Dixon and C. A. Hall, "Introduction: Basic Principles," *Fluid Mech. Thermodyn. Turbomach.*, p. 9, Jan. 2014, doi: 10.1016/B978-0-12-415954-9.00001-2.

[88] P. W. Windes, D. K. Tafti, and B. Behkam, "Computational Model of Human Capillary Hydrodynamics," *ASME 2016 Fluids Engineering Division Summer Meeting collocated with the ASME 2016 Heat Transfer Summer Conference and the ASME 2016 14th International Conference on Nanochannels, Microchannels, and Minichannels*. Jul. 10, 2016, doi: 10.1115/FEDSM2016-7858.

[89] B. Munson, D. Young, and T. Okiishi, *Fundamentals of Fluid Mechanics*, 6th ed.

Wiley, 2009.

[90] S. M. Choi, W. H. Kim, D. Côté, C.-W. Park, and H. Lee, “Blood cell assisted in vivo Particle Image Velocimetry using the confocal laser scanning microscope.,” *Opt. Express*, vol. 19, no. 5, pp. 4357–68, Feb. 2011, doi: 10.1364/OE.19.004357.

[91] U. Morbiducci *et al.*, “On the importance of blood rheology for bulk flow in hemodynamic models of the carotid bifurcation,” *J. Biomech.*, vol. 44, no. 13, pp. 2427–2438, Sep. 2011, doi: 10.1016/J.JBIOMECH.2011.06.028.

[92] M. G. Levitzky, “Using the pathophysiology of obstructive sleep apnea to teach cardiopulmonary integration,” *Adv. Physiol. Educ.*, vol. 32, no. 3, pp. 196–202, Sep. 2008, doi: 10.1152/advan.90137.2008.

[93] A. C. Guyton and J. E. Hall, *Textbook of Medical Physiology*, 6th ed. Philadelphia, USA: W.B.Sounders Company, 1981.

[94] V. O. Kheyfets *et al.*, “Patient-specific computational modeling of blood flow in the pulmonary arterial circulation,” *Comput. Methods Programs Biomed.*, vol. 120, no. 2, pp. 88–101, Jul. 2015, doi: 10.1016/J.CMPB.2015.04.005.

[95] X. Yao *et al.*, “Carotid geometry as a predictor of in-stent neointimal hyperplasia: A computational fluid dynamics study,” *Circ. J.*, vol. 83, no. 7, pp. 1472–1479, 2019, doi: 10.1253/circj.CJ-18-1152.

[96] L. C. Sousa *et al.*, “Computational simulation of carotid stenosis and flow dynamics based on patient ultrasound data – A new tool for risk assessment and surgical planning,” *Adv. Med. Sci.*, vol. 61, no. 1, pp. 32–39, Mar. 2016, doi: 10.1016/J.ADVMS.2015.07.009.

[97] G. J. Harrison *et al.*, “Closure technique after carotid endarterectomy influences local hemodynamics,” *J. Vasc. Surg.*, vol. 60, no. 2, pp. 418–427, Aug. 2014, doi: 10.1016/J.JVS.2014.01.069.

[98] A. R. Pries, D. Neuhaus, and P. Gaehtgens, “Blood viscosity in tube flow: Dependence on diameter and hematocrit,” *Am. J. Physiol. - Hear. Circ. Physiol.*, vol. 263, no. 6 32-6, 1992, doi: 10.1152/ajpheart.1992.263.6.h1770.

APPENDIX

App 1 – Tables

Table 2: Cross-sectional area, diameter and the viscosity obtained from 10 equally spaced planes placed along the segment with H_t of 0.45

	Cross-Sectional Area (μm)	Average Diameter (μm)	Relative Apparent Viscosity	Average Viscosity of Two Consecutive Planes (cP)
Inlet	30.3188	6.2131	1.2604	1.3187
P101	32.8817	6.4704	1.2514	1.3126
P102	39.8257	7.1209	1.2488	1.3218
P103	51.2110	8.0749	1.2690	1.4416
P104	19.5153	4.9847	1.4770	1.5807
P105	18.4983	4.8531	1.5340	1.4610
P106	34.2284	6.6016	1.2489	5.1585
P107	5.2800	2.5928	8.5769	5.3304
P108	17.8652	4.7693	1.5762	1.4871
P109	31.2284	6.3057	1.2564	3.8379
Outlet	6.6416	2.9080	6.0538	

Table 3: Cross-sectional area, diameter and the viscosity obtained from 20 equally spaced planes placed along the segment with H_t of 0.45

	Cross-Sectional Area (μm)	Average Diameter (μm)	Relative Apparent Viscosity	Average Viscosity of Two Consecutive Planes (cP)
Inlet	30.3188	6.2131	1.2604	1.3199
P101	32.0454	6.3876	1.2536	1.3151
P102	32.8818	6.4704	1.2514	1.3390
P103	25.8621	5.7383	1.2991	1.3376
P104	39.8258	7.1209	1.2488	1.3116
P105	33.7666	6.5569	1.2496	1.3223
P106	51.2110	8.0749	1.2690	1.3499
P107	25.6307	5.7126	1.3023	1.4591
P108	19.5153	4.9847	1.4770	2.1993
P109	11.1792	3.7728	2.7122	2.2292
P110	18.4983	4.8531	1.5340	1.4948
P111	24.9148	5.6323	1.3133	1.3452
P112	34.2284	6.6016	1.2489	1.3514
P113	24.2417	5.5557	1.3253	5.1986
P114	5.2800	2.5928	8.5769	7.7791
P115	6.5129	2.8797	6.2404	4.1037
P116	17.8651	4.7693	1.5762	1.6669
P117	17.5587	4.7283	1.5988	1.4990
P118	31.2284	6.3057	1.2564	1.8052
P119	13.1143	4.0863	2.1821	4.3239
Outlet	6.6416	2.9080	6.0538	

Table 4: Cross-sectional area, diameter and the viscosity obtained from 30 equally spaced planes placed along the segment with H_t of 0.45

	Area (μm)	Average Diameter (μm)	Relative Apparent Viscosity	Average Viscosity of Two Consecutive Planes (cP)
Inlet	30.3188	6.2131	1.2604	1.3165
P101	37.3998	6.9006	1.2473	1.3123
P102	32.5111	6.4338	1.2523	1.3144
P103	32.8818	6.4704	1.2514	1.3223
P104	29.1203	6.0891	1.2673	1.3392
P105	27.1852	5.8833	1.2834	1.3294
P106	39.8258	7.1209	1.2488	1.3114
P107	40.1437	7.1493	1.2491	1.3110
P108	39.1145	7.0571	1.2481	1.3215
P109	51.2110	8.0749	1.2690	1.3236
P110	32.5804	6.4407	1.2521	1.3153
P111	32.1540	6.3984	1.2533	1.4334
P112	19.5153	4.9847	1.4770	1.9195
P113	13.1277	4.0884	2.1793	2.1041
P114	15.2479	4.4062	1.8286	1.7653
P115	18.4983	4.8531	1.5340	1.8925
P116	13.6769	4.1730	2.0707	1.7446
P117	32.4655	6.4293	1.2524	1.3132
P118	34.2284	6.6016	1.2489	1.3292
P119	27.2362	5.8888	1.2829	1.4407
P120	19.8369	5.0256	1.4613	5.2701
P121	5.2800	2.5928	8.5769	7.7486
P122	6.5523	2.8884	6.1823	6.6237
P123	6.3853	2.8513	6.4342	4.2055
P124	17.8651	4.7693	1.5762	1.7231
P125	16.3327	4.5602	1.7059	1.6383
P126	20.9525	5.1650	1.4145	1.4023
P127	31.2284	6.3057	1.2564	1.4223
P128	20.0252	5.0494	1.4527	2.1988
P129	11.1132	3.7616	2.7354	4.6144
Outlet	6.6416	2.9080	6.0538	

Table 5: Cross-sectional area, diameter and the viscosity obtained from 10 planes placed at varying distances along the segment with H_t of 0.45

	Cross-sectional Area (μm)	Average Diameter (μm)	Relative Apparent Viscosity	Average Viscosity of Two Consecutive Planes (cP)
Inlet	30.3188	6.2131	1.2604	1.3171
P101	39.3752	7.0805	1.2484	1.5590
P102	16.1828	4.5392	1.7212	2.5123
P103	10.2886	3.6194	3.0642	5.1046
P104	6.2447	2.8197	6.6588	5.9197
P105	7.8955	3.1706	4.6169	3.8962
P106	10.9240	3.7295	2.8044	2.2749
P107	18.5832	4.8642	1.5287	1.4595
P108	32.8887	6.4711	1.2513	1.9608
P109	11.8990	3.8923	2.4835	4.4821
Outlet	6.6416	2.9080	6.0538	

Table 6: Cross-sectional area, diameter and the viscosity obtained from 20 planes placed at varying distances along the segment with H_t of 0.45

	Cross-sectional Area (μm)	Average Diameter (μm)	Relative Apparent Viscosity	Average Viscosity of Two Consecutive Planes (cP)
Inlet	30.3188	6.2131	1.2604	1.3171
P101	39.3752	7.0805	1.2484	1.5590
P102	16.1828	4.5392	1.7212	2.2778
P103	11.4608	3.8200	2.6175	2.0478
P104	27.2167	5.8867	1.2831	2.2823
P105	10.2886	3.6194	3.0642	3.5625
P106	9.0602	3.3964	3.7216	4.6502
P107	7.3782	3.0650	5.1360	6.2472
P108	6.1815	2.8055	6.7635	8.0113
P109	5.3139	2.6011	8.4962	7.9564
P110	6.2447	2.8197	6.6588	6.7175
P111	6.5838	2.8953	6.1365	6.3108
P112	6.7642	2.9347	5.8840	5.5130
P113	7.8955	3.1706	4.6169	3.8962
P114	10.9240	3.7295	2.8044	2.2749
P115	18.5832	4.8642	1.5287	1.6954
P116	16.3861	4.5677	1.7006	1.5498
P117	32.8887	6.4711	1.2513	1.3989
P118	20.9882	5.1694	1.4132	2.0458
P119	11.8990	3.8923	2.4835	4.4821
Outlet	6.6416	2.9080	6.0538	

Table 7: Cross-sectional area, diameter and the viscosity obtained from 30 planes placed at varying distances along the segment with H_t of 0.45

	Cross-Sectional Area (μm)	Average Diameter (μm)	Relative Apparent Viscosity	Average Viscosity of Two Consecutive Planes (cP)
Inlet	30.3188	6.2131	1.2604	1.3165
P101	37.3254	6.8938	1.2473	1.3204
P102	29.0513	6.0819	1.2678	1.3204
P103	37.0150	6.8651	1.2472	1.3102
P104	39.3752	7.0805	1.2484	1.3204
P105	50.1376	7.9898	1.2666	1.3375
P106	27.4322	5.9100	1.2810	1.3334
P107	30.6732	6.2493	1.2588	2.0350
P108	11.4608	3.8200	2.6175	3.1553
P109	9.6202	3.4998	3.3926	2.4547
P110	27.2167	5.8867	1.2831	1.4278
P111	20.3947	5.0958	1.4366	2.3629
P112	10.2886	3.6194	3.0642	5.1595
P113	6.1815	2.8055	6.7635	7.9507
P114	5.3632	2.6132	8.3808	7.6215
P115	6.5838	2.8953	6.1365	6.4728
P116	6.5452	2.8868	6.1927	6.3403
P117	6.7642	2.9347	5.8840	5.5130
P118	7.8955	3.1706	4.6169	3.8962
P119	10.9240	3.7295	2.8044	2.2749
P120	18.5832	4.8642	1.5287	1.6954
P121	16.3861	4.5677	1.7006	1.7402
P122	17.3624	4.7017	1.6141	1.5708
P123	22.0507	5.2987	1.3779	1.3803
P124	32.8887	6.4711	1.2513	1.3247
P125	28.4883	6.0227	1.2718	1.4097
P126	20.9882	5.1694	1.4132	1.6839
P127	15.5259	4.4461	1.7942	2.2458
P128	11.8990	3.8923	2.4835	3.0899
P129	9.6029	3.4967	3.4020	4.9643
Outlet	6.6416	2.9080	6.0538	

Table 8: Cross-sectional area, diameter, the constant C and the viscosity obtained from 30 planes placed at varying distances along the segment with H_t of 0.40

	Cross-Sectional Area (μm)	Average Diameter (μm)	Constant C value	Relative Apparent Viscosity
Inlet	30.3188	6.2131	0.922239	1.2924
P101	37.3254	6.8938	0.752446	1.2787
P102	29.0513	6.0819	0.939223	1.2994
P103	37.0150	6.8651	0.763222	1.2788
P104	39.3752	7.0805	0.672787	1.2790
P105	50.1376	7.9898	0.051810	1.2898
P106	27.4322	5.9100	0.956454	1.3118
P107	30.6732	6.2493	0.916875	1.2908
P108	11.4608	3.8200	0.999754	2.5597
P109	9.6202	3.4998	0.999913	3.2831
P110	27.2167	5.8867	0.958413	1.3138
P111	20.3947	5.0958	0.992413	1.4574
P112	10.2886	3.6194	0.999871	2.9766
P113	6.1815	2.8055	0.999994	6.4292
P114	5.3632	2.6132	0.999997	7.9387
P115	6.5838	2.8953	0.999991	5.8440
P116	6.5452	2.8868	0.999991	5.8966
P117	6.7642	2.9347	0.999989	5.6084
P118	7.8955	3.1706	0.999973	4.4257
P119	10.9240	3.7295	0.999815	2.7341
P120	18.5832	4.8642	0.995631	1.5434
P121	16.3861	4.5677	0.997932	1.7039
P122	17.3624	4.7017	0.997082	1.6231
P123	22.0507	5.2987	0.987951	1.4025
P124	32.8887	6.4711	0.876423	1.2835
P125	28.4883	6.0227	0.945743	1.3032
P126	20.9882	5.1694	0.991006	1.4355
P127	15.5259	4.4461	0.998499	1.7912
P128	11.8990	3.8923	0.999692	2.4346
P129	9.6029	3.4967	0.999914	3.2918
Outlet	6.6416	2.9080	0.999990	

App 2 – Codes

```
/************************************************ *********************
UDF for 10 equally spaced planes with average viscosity
************************************************ *********************/

#include "udf.h"
DEFINE_PROPERTY(cell_viscosity, cell, thread)
{
        real xc[ND_ND];
        real mu;

                        C_CENTROID(xc, cell, thread);

                        if (xc[0]< 0.0000130945410167)
                        {
                        mu = 1.31868999540353e-3;
                        }

                        else if (xc[0] <= 0.0000261896475704)
                        {
                        mu = 1.31256279965800e-3;
                        }

                        else if (xc[0] <= 0.0000392847541241)
                        {
                        mu = 1.32181477809123e-3;
                        }

                        else if (xc[0] <= 0.0000523798606778)
                        {
                        mu = 1.44162756299246e-3;
                        }

                        else if (xc[0] <= 0.0000654749672315)
                        {
                        mu = 1.58074500864957e-3;
                        }

                        else if (xc[0] <= 0.0000785700737852)
                        {
                        mu = 1.46100130778828e-3;
                        }

                        else if (xc[0] <= 0.0000916651803389)
                        {
                        mu = 5.15853504135248e-3;
                        }

                        else if (xc[0] <= 0.0001047602868926)
                        {
                        mu = 5.33036961880770e-3;
                        }

                        else if (xc[0] <= 0.0001178553934463)
                        {
                        mu = 1.48713140398798e-3;
                        }
```

```
                        else
                                {
                        mu = 3.83789527309031e-3;
                                }
return mu;

        }


/*********************************************** ********************
UDF for 20 equally spaced planes with average viscosity
*********************************************** *********************/

#include "udf.h"
DEFINE_PROPERTY(cell_viscosity, cell, thread)
{
        real xc[ND_ND];
        real mu;

                        C_CENTROID(xc, cell, thread);

                        if (xc[0]< 0.00000654698774)
                        {
                        mu = 1.31987081463054e-3;
                        }

                        else if (xc[0] <= 0.00001309454102)
                        {
                        mu = 1.31510741223854e-3;
                        }

                        else if (xc[0] <= 0.00001964209429)
                        {
                        mu = 1.33899699166047e-3;
                        }

                        else if (xc[0] <= 0.00002618964757)
                        {
                        mu = 1.33763319830695e-3;
                        }

                        else if (xc[0] <= 0.00003273720085)
                        {
                        mu = 1.31163581609860e-3;
                        }

                        else if (xc[0] <= 0.00003928475412)
                        {
                        mu = 1.32225158788536e-3;
                        }

                        else if (xc[0] <= 0.0000458323074)
                        {
                        mu = 1.34993989541695e-3;
                        }

                        else if (xc[0] <= 0.00005237986068)
```

```
                        {
                        mu = 1.45913690853142e-3;
                        }

                        else if (xc[0] <= 0.00005892741395)
                        {
                        mu = 2.19931872811103e-3;
                        }

                        else if (xc[0] <= 0.00006547496723)
                        {
                        mu = 2.22924079559994e-3;
                        }

                        else if (xc[0] <= 0.00007202252051)
                        {
                        mu = 1.49484013675304e-3;
                        }

                        else if (xc[0] <= 0.00007857007379)
                        {
                        mu = 1.34517436840284e-3;
                        }
                        else if (xc[0] <= 0.00008511762706)
                        {
                        mu = 1.35144919188195e-3;
                        }
                        else if (xc[0] <= 0.00009166518034)
                        {
                        mu = 5.19864705885009e-3;
                        }
                        else if (xc[0] <= 0.00009821273362)
                        {
                        mu =  7.77907790659432e-3;
                        }
                        else if (xc[0] <= 0.00010476028689)
                        {
                        mu = 4.1037146170814e-3;
                        }
                        else if (xc[0] <= 0.00011130784017)
                        {
                        mu = 1.66686651395083e-3;
                        }
                        else if (xc[0] <= 0.00011785539345)
                        {
                        mu = 1.49899158864402e-3;
                        }
                        else if (xc[0] <= 0.00012440294672)
                        {
                        mu = 1.80524801181297e-3;
                        }
                        else
                                {
                        mu = 4.32388680622210e-3;
                                }
return mu;

        }
```

```
/**********************************************  ********************
UDF for 30 equally spaced planes with average viscosity
**********************************************  *********************/

#include "udf.h"
DEFINE_PROPERTY(cell_viscosity, cell, thread)
{
        real xc[ND_ND];
        real mu;

                        C_CENTROID(xc, cell, thread);

                        if (xc[0]< 0.00000436446998)
                        {
                        mu = 1.31654962e-3;
                        }

                        else if (xc[0] <= 0.0000087295055)
                        {
                        mu = 1.31227037e-3;
                        }

                        else if (xc[0]< 0.00001309454102)
                                {
                                mu = 1.31441074e-3;
                                }

                        else if (xc[0] <= 0.00001745957653)
                        {
                        mu = 1.3223083e-3;
                        }

                        else if (xc[0] <= 0.00002182461205)
                        {
                        mu = 1.33915004e-3;
                        }

                        else if (xc[0] <= 0.00002618964757)
                        {
                        mu = 1.32940455e-3;
                        }

                        else if (xc[0] <= 0.00003055468309)
                        {
                        mu = 1.31136565e-3;
                        }

                        else if (xc[0] <= 0.00003491971861)
                        {
                        mu = 1.31104206e-3;
                        }

                        else if (xc[0] <= 0.00003928475412)
                        {
                        mu = 1.32149118e-3;
                        }
```

```
else if (xc[0] <= 0.00004364978964)
{
mu = 1.32356757e-3;
}

else if (xc[0] <= 0.00004801482516)
{
mu = 1.31532485e-3;
}

else if (xc[0] <= 0.00005237986068)
{
mu = 1.43338485e-3;
}

else if (xc[0] <= 0.0000567448962)
{
mu = 1.91953910e-3;
}

else if (xc[0] <= 0.00006110993171)
{
mu = 2.10411754e-3;
}

else if (xc[0] <= 0.00006547496723)
{
 mu = 1.76532345e-3;
}

else if (xc[0] <= 0.00006984000275)
{
mu = 1.89246051e-3;
}

else if (xc[0] <= 0.00007420503827)
{
mu = 1.74463907e-3;
}

else if (xc[0] <= 0.00007857007379)
{
mu = 1.31317987e-3;
}

else if (xc[0] <= 0.00008293510930)
{
mu = 1.32920094e-3;
}


else if (xc[0] <= 0.00008730014482)
{
mu = 1.44073919e-3;
}

else if (xc[0] <= 0.00009166518034)
```

```
                        {
                        mu = 5.27007330e-3;
                        }

                        else if (xc[0] <= 0.00009603021586)
                        {
                        mu = 7.74859532e-3;
                        }

                        else if (xc[0] <= 0.00010039525137)
                        {
                        mu = 6.62368519e-3;
                        }

                        else if (xc[0] <= 0.00010476028689)
                        {
                        mu = 4.20545948e-3;
                        }

                        else if (xc[0] <= 0.00010912532241)
                        {
                        mu = 1.72312475e-3;
                        }

                        else if (xc[0] <= 0.00011349035793)
                        {
                        mu = 1.63825922e-3;
                        }

                        else if (xc[0] <= 0.00011785539345)
                        {
                        mu = 1.40226588e-3;
                        }

                        else if (xc[0] <= 0.00012222042896)
                        {
                        mu = 1.42227843e-3;
                        }

                        else if (xc[0] <= 0.00012658546448)
                        {
                        mu = 2.19875916e-3;
                        }

                        else
                        {
                        mu = 4.61437600e-3;
                        }

return mu;

        }
```

```
/********************************************** *********************
UDF for 10 planes placed at varying distances
along the segment with average viscosity
********************************************** *********************/

#include "udf.h"
DEFINE_PROPERTY(cell_viscosity, cell, thread)
{
        real xc[ND_ND];
        real mu;
                        C_CENTROID(xc, cell, thread);

                        if (xc[0]< 0.000035)
                        {
                        mu = 1.31711299e-3;
                        }

                        else if (xc[0] <= 0.0000535)
                        {
                        mu = 1.55899287e-3;
                        }

                        else if (xc[0] <= 0.00009)
                        {
                        mu = 2.51229699e-3;
                        }


                        else if (xc[0] <= 0.000093)
                        {
                        mu = 5.10455630e-3;
                        }

                        else if (xc[0] <= 0.000102)
                        {
                        mu = 5.91971644e-3;
                        }


                        else if (xc[0] <= 0.000103)
                        {
                        mu = 3.89618457e-3;
                        }

                        else if (xc[0] <= 0.000105)
                        {
                        mu = 2.27491665e-3;
                        }

                        else if (xc[0] <= 0.000119)
                        {
                        mu = 1.45953748e-3;
                        }

                        else if (xc[0] <= 0.000125)
                        {
                        mu = 1.96081701e-3;
                        }
```

```
                        else
                        {
                        mu = 4.4821292e-3;
                        }

return mu;

        }



/********************************************** ********************
UDF for 20 planes placed at varying distances
along the segment with average viscosity
********************************************** *********************/

#include "udf.h"
DEFINE_PROPERTY(cell_viscosity, cell, thread)
{

        real xc[ND_ND];
        real mu;

                        C_CENTROID(xc, cell, thread);

                        if (xc[0]< 0.000035)
                        {
                        mu = 1.31711299e-3;
                        }

                        else if (xc[0] <= 0.0000535)
                        {
                        mu = 1.55899287e-3;
                        }

                        else if (xc[0] <= 0.00006)
                        {
                        mu = 2.2778062e-3;
                        }

                        else if (xc[0] <= 0.000083)
                        {
                        mu = 2.04783557e-3;
                        }

                        else if (xc[0] <= 0.00009)
                        {
                        mu = 2.28232636e-3;
                        }

                        else if (xc[0] <= 0.0000903)
                        {
                        mu = 3.56253207e-3;
                        }

                        else if (xc[0] <= 0.0000907)
```

```
{
mu = 4.65024567e-3;
}

else if (xc[0] <= 0.000091)
{
mu = 6.24722878e-3;
}

else if (xc[0] <= 0.0000915)
{
mu = 8.01130914e-3;
}

else if (xc[0] <= 0.000093)
{
mu = 7.95635027e-3;
}

else if (xc[0] <= 0.000094)
{
mu = 6.71751366e-3;
}

else if (xc[0] <= 0.000101)
{
mu = 6.31075281e-3;
}

else if (xc[0] <= 0.000102)
{
mu = 5.51295559e-3;
}


else if (xc[0] <= 0.000103)
{
mu = 3.89618457e-3;
}

else if (xc[0] <= 0.000105)
{
mu = 2.27491665e-3;
}

else if (xc[0] <= 0.000109)
{
mu = 1.69542344e-3;
}

else if (xc[0] <= 0.000119)
{
mu = 1.54979566e-3;
}

else if (xc[0] <= 0.000122)
{
mu = 1.39889462e-3;
```

```
                        }

                        else if (xc[0] <= 0.000125)
                        {
                        mu = 2.04580194e-3;
                        }

                        else
                        {
                        mu = 4.4821292e-3;
                        }

return mu;

        }



/********************************************** ********************
UDF for 30 planes placed at varying distances
along the segment with average viscosity
********************************************** *********************/

#include "udf.h"
DEFINE_PROPERTY(cell_viscosity, cell, thread)
{
        real xc[ND_ND];
        real mu;

                        C_CENTROID(xc, cell, thread);

                        if (xc[0]< 0.0000037)
                        {
                        mu = 1.316541982198e-3;
                        }

                        else if (xc[0] <= 0.0000175)
                        {
                        mu = 1.320402423246e-3;
                        }

                        else if (xc[0] <= 0.000025)
                        {
                        mu = 1.32038264895e-3;
                        }

                        else if (xc[0]< 0.000035)
                        {
                        mu = 1.310181800273e-3;
                        }

                        else if (xc[0] <= 0.00004)
                        {
                        mu = 1.320375214342e-3;
                        }

                        else if (xc[0] <= 0.0000465)
                        {
```

```
mu = 1.33750044709e-3;
}

else if (xc[0] <= 0.00005)
{
mu = 1.333360162384e-3;
}

else if (xc[0] <= 0.00006)
{
mu = 2.03504825943e-3;
}

else if (xc[0] <= 0.000067)
{
mu =  3.15529882012e-3;
}

else if (xc[0] <= 0.000083)
{
mu = 2.454735147968e-3;
}

else if (xc[0] <= 0.000087)
{
mu = 1.427849313684e-3;
}

else if (xc[0] <= 0.00009)
{
mu = 2.362903775675e-3;
}

else if (xc[0] <= 0.000091)
{
mu = 5.159515179216e-3;
}

else if (xc[0] <= 0.000092)
{
mu = 7.950724690345e-3;
}

else if (xc[0] <= 0.000094)
{
mu = 7.621547683974e-3;
}

else if (xc[0] <= 0.000097)
{
mu = 6.472836916706e-3;
}

else if (xc[0] <= 0.000101)
{
mu = 6.340294200288e-3;
}
```

```
else if (xc[0] <= 0.000102)
{
mu = 5.512955593449e-3;
}

else if (xc[0] <= 0.000103)
{
mu = 3.896184565242e-3;
}

else if (xc[0] <= 0.000105)
{
mu = 2.274916647249e-3;
}

else if (xc[0] <= 0.000109)
{
mu = 1.695423443076e-3;
}

else if (xc[0] <= 0.000111)
{
mu = 1.740230563839e-3;
}

else if (xc[0] <= 0.000114)
{
mu = 1.570773988828e-3;
}

else if (xc[0] <= 0.000119)
{
mu = 1.380339083565e-3;
}

else if (xc[0] <= 0.0001205)
{
mu = 1.324667589258e-3;
}

else if (xc[0] <= 0.000122)
{
mu = 1.409652520298e-3;
}

else if (xc[0] <= 0.0001235)
{
mu = 1.68389464647e-3;
}

else if (xc[0] <= 0.000125)
{
mu = 2.245817035147e-3;
}

else if (xc[0] <= 0.00013)
{
mu = 3.089891619071e-3;
```

```
                        }

                        else if (xc[0] <= 0.000131)
                        {
                        mu = 4.964296487642e-3;
                        }

                        else
                        {
                        mu = 3.5e-3;
                        }
return mu;

        }
```

```
/********************************************** ********************
UDF for 10 equally spaced planes with linear
correlation for the viscosity
********************************************** ********************/

#include "udf.h"
DEFINE_PROPERTY(cell_viscosity, cell, thread)
{
        real xc[ND_ND];
        real mu;

                        C_CENTROID(xc, cell, thread);

                if (xc[0]< 0.0000130945410167)
                {
                mu = 0.0013234529863624-0.727508764050356*xc[0];
                }

                else if (xc[0] <= 0.0000261896475704)
                {
                mu = 0.00131665406222704-0.208290554975234*xc[0];
                }

                else if (xc[0] <= 0.0000392847541241)
                {
                mu = 1.62133419174058*xc[0]+0.00126873683492447;
                }

                else if (xc[0] <= 0.0000523798606778)
                {
                mu = 16.6775295110747*xc[0]+0.000677257903760007;
                }

                else if (xc[0] <= 0.0000654749672315)
                {
                mu = 4.5697119572572*xc[0]+0.00131146370034119;
                }
```

```
                else if (xc[0] <= 0.0000785700737852)
                {
                mu = 0.00310729384894137-22.8580245431776*xc[0];
                }

                else if (xc[0] <= 0.0000916651803389)
                {
                mu = 587.57794008373*xc[0]-0.0448547049329345;
                }

                else if (xc[0] <= 0.0001047602868926)
                {
                mu = 0.0604605015059384-561.333850080286*xc[0];
                }

                else if (xc[0] <= 0.0001178553934463)
                {
                mu = 0.00434099062900627-25.6393370014339*xc[0];
                }

                else if (xc[0] <= 0.0001309505)
                {
                mu = 384.668697986022*xc[0]-0.0440160242686185;
                }
                        else
                                {
                        mu = 3.5e-3;
                                }
return mu;

        }



/********************************************** ********************
UDF for 20 equally spaced planes with linear
correlation for the viscosity
********************************************** *********************/

#include "udf.h"
DEFINE_PROPERTY(cell_viscosity, cell, thread)
{
        real xc[ND_ND];
        real mu;

                        C_CENTROID(xc, cell, thread);

                if (xc[0]< 0.00000654698774)
                {
                mu = 0.00132345277911736-1.09432740702844*xc[0];
                }

                else if (xc[0] <= 0.00001309454102)
                {
                mu = 0.00131864966501529-0.36069015386462*xc[0];
                }

                else if (xc[0] <= 0.00001964209429)
```

```
{
mu = 7.65794411016682*xc[0]+0.00121364932972055;
}

else if (xc[0] <= 0.00002618964757)
{
mu = 0.00152266797545227-8.07452520646002*xc[0];
}

else if (xc[0] <= 0.00003273720085)
{
mu = 0.133426940208114*xc[0]+0.00130770460145961;
}

else if (xc[0] <= 0.00003928475412)
{
mu = 3.10924144646173*xc[0]+0.00121028476427604;
}

else if (xc[0] <= 0.0000458323074)
{
mu = 5.34836289258879*xc[0]+0.00112232142882012;
}

else if (xc[0] <= 0.00005237986068)
{
mu = 28.0066961135137*xc[0]+0.000083837735467054;
}

else if (xc[0] <= 0.00005892741395)
{
mu = 198.087476423082*xc[0]-0.00882496984149383;
}

else if (xc[0] <= 0.00006547496723)
{
mu = 0.0139820329676501-188.948052210428*xc[0];
}

else if (xc[0] <= 0.00007202252051)
{
mu = 0.00392718422100867-35.3802205333104*xc[0];
}

else if (xc[0] <= 0.00007857007379)
{
mu = 0.00212342398436546-10.3358285310509*xc[0];
}
else if (xc[0] <= 0.00008511762706)
{
mu = 12.2525211620004*xc[0]+0.000348655682188091;
}
else if (xc[0] <= 0.00009166518034)
{
mu = 1162.9033584588*xc[0]-0.0975920131631185;
}
else if (xc[0] <= 0.00009821273362)
{
```

```
                mu = 0.0433518610322023-374.691109500983*xc[0];
                }
                else if (xc[0] <= 0.00010476028689)
                {
                mu = 0.080013248616596-747.976591261853*xc[0];
                }
                else if (xc[0] <= 0.00011130784017)
                {
                mu = 3.6227838072667*xc[0]+0.00127548245801029;
                }
                else if (xc[0] <= 0.00011785539345)
                {
                mu = 0.00778968938728449-54.9014577854646*xc[0];
                }
                else if (xc[0] <= 0.00012440294672)
                {
                mu = 148.449814139504*xc[0]-0.0161763547739906;
                }

                else if (xc[0] <= 0.0001309505)
                {
                mu = 620.887581689141*xc[0]-0.0749490051989838;
                }
                        else
                                {
                        mu = 4.3e-3;
                                }
return mu;

        }


/********************************************** ********************
UDF for 30 equally spaced planes with linear
correlation for the viscosity
********************************************** *********************/


#include "udf.h"
DEFINE_PROPERTY(cell_viscosity, cell, thread)
{
        real xc[ND_ND];
        real mu;

                        C_CENTROID(xc, cell, thread);

                if (xc[0]< 0.00000436446998)
                {
                mu = 0.00132345160908317-3.1632180187825*xc[0];
                }

                else if (xc[0] <= 0.0000087295055)
                {
                mu = 1.20252286056999*xc[0]+0.00130439746407478;
                }

                else if (xc[0]< 0.00001309454102)
                {
```

```
mu = 0.00131683137054559-0.221831184548986*xc[0];
}

else if (xc[0] <= 0.00001745957653)
{
mu = 3.84038250355494*xc[0]+0.00126363854677471;
}

else if (xc[0] <= 0.00002182461205)
{
mu = 3.87627681893411*xc[0]+0.00126301184722835;
}

else if (xc[0] <= 0.00002618964757)
{
mu = 0.00152966076244716-8.34153097567463*xc[0];
}

else if (xc[0] <= 0.00003055468309)
{
mu = 0.0763542469409275*xc[0]+0.00130919931518214;
}

else if (xc[0] <= 0.00003491971861)
{
mu = 0.00131839550696581-0.224620623476622*xc[0];
}

else if (xc[0] <= 0.00003928475412)
{
mu = 5.01226896090016*xc[0]+0.00113552479628773;
}
else if (xc[0] <= 0.00004364978964)
{
mu = 0.00149196190231892-4.06089730971994*xc[0];
}

else if (xc[0] <= 0.00004801482516)
{
mu = 0.284196541887476*xc[0]+0.0013022994697302;
}

else if (xc[0] <= 0.00005237986068)
{
mu = 53.8092892769862*xc[0]-0.00126769849961836 ;
}

else if (xc[0] <= 0.0000567448962)
{
mu = 168.939987686515*xc[0]-0.00729822844230056;
}

else if (xc[0] <= 0.00006110993171)
{
mu = 0.00707574401143322-84.3686517913345*xc[0];
}

else if (xc[0] <= 0.00006547496723)
```

```
{
  mu = 0.00625036567846542-70.8622002232871*xc[0];
}

else if (xc[0] <= 0.00006984000275)
{
mu = 129.114676024446*xc[0]-0.00684311374061268;
}

else if (xc[0] <= 0.00007420503827)
{
mu = 0.0159218727226828-196.844452940443*xc[0];
}

else if (xc[0] <= 0.00007857007379)
{
mu = 0.00137767362649113-0.844296680545683*xc[0];
}

else if (xc[0] <= 0.00008293510930)
{
mu = 8.18493295602079*xc[0]+0.000668246387679244;
}

else if (xc[0] <= 0.00008730014482)
{
mu = 42.9203815505263*xc[0]-0.0022125418380906;
}

else if (xc[0] <= 0.00009166518034)
{
mu = 1711.62850491535*xc[0]-0.14789100267015;
}

else if (xc[0] <= 0.00009603021586)
{
mu = 0.0618051858280132-576.003371445646*xc[0];
}

else if (xc[0] <= 0.00010039525137)
{
mu = 60.584823741789*xc[0]+0.000673484030235951;
}

else if (xc[0] <= 0.00010476028689)
{
mu = 0.12407609683014-1168.58300158804*xc[0];
}

else if (xc[0] <= 0.00010912532241)
{
mu = 31.2109336512341*xc[0]-0.00161466003440804;
}

else if (xc[0] <= 0.00011349035793)
{
mu = 0.00944040051787628-70.0951638533287*xc[0];
}
```

```
                else if (xc[0] <= 0.00011785539345)
                {
                mu = 0.00580174267547394-38.0337807652021*xc[0];
                }

                else if (xc[0] <= 0.00012222042896)
                {
                mu = 47.203259750801*xc[0]-0.0042439022710532;
                }

                else if (xc[0] <= 0.00012658546448)
                {
                mu = 308.569666347182*xc[0]-0.0361882166009967;
                }

                else if (xc[0] <= 0.0001309505)
                {
                mu = 798.233167413034*xc[0]-0.0981724983223205;
                }

                else
                {
                mu = 4.3e-3;
                }

return mu;

        }


/********************************************** ********************
UDF for 10 planes placed at varying lengths with
linear correlation for the viscosity
********************************************** ********************/


#include "udf.h"
DEFINE_PROPERTY(cell_viscosity, cell, thread)
{
        real xc[ND_ND];
        real mu;

                        C_CENTROID(xc, cell, thread);

                if (xc[0]< 0.000035)
                {
                mu = 0.00132345319310417-0.362303145833309*xc[0];
                }

                else if (xc[0] <= 0.0000535)
                {
                mu = 26.8346255135135*xc[0]+0.000371560690027027;
                }

                else if (xc[0] <= 0.00009)
                {
                mu = 38.6347306027397*xc[0]-0.000259744932246575;
```

```
                }


                else if (xc[0] <= 0.000093)
                {
                mu = 1258.11698866667*xc[0]-0.110013148158;
                }

                else if (xc[0] <= 0.000102)
                {
                mu = 0.0291467156053333-238.225632444444*xc[0];
                }

                else if (xc[0] <= 0.000103)
                {
                mu = 0.198957073318-1903.033061*xc[0];
                }

                else if (xc[0] <= 0.000105)
                {
                mu = 0.0719290609475-669.7513875*xc[0];
                }

                else if (xc[0] <= 0.000119)
                {
                mu = 0.0037895820275-20.8039692142857*xc[0];
                }

                else if (xc[0] <= 0.000125)
                {
                mu = 215.635773166667*xc[0]-0.0243467473158333;
                }

                else if (xc[0] <= 0.001309505)
                {
                mu = 629.99911553651*xc[0]-0.076142165112063;
                }


                else
                {
                mu = 4.3e-3;
                }

return mu;

        }


/********************************************** ********************
UDF for 20 planes placed at varying lengths with
linear correlation for the viscosity
********************************************** *********************/


#include "udf.h"
DEFINE_PROPERTY(cell_viscosity, cell, thread)
{
```

```
real xc[ND_ND];
real mu;

              C_CENTROID(xc, cell, thread);

        if (xc[0]< 0.000035)
        {
        mu = 0.00132345319310417-0.362303145833309*xc[0];
        }

        else if (xc[0] <= 0.0000535)
        {
        mu = 26.8346255135135*xc[0]+0.000371560690027027;
        }

        else if (xc[0] <= 0.00006)
        {
        mu = 144.797859538462*xc[0]-0.00593947233030769;
        }

        else if (xc[0] <= 0.000083)
        {
        mu = 0.00640351405243478-60.918580173913*xc[0];
        }

        else if (xc[0] <= 0.00009)
        {
        mu = 267.158417714286*xc[0]-0.0208268767722857;
        }

        else if (xc[0] <= 0.0000903)
        {
        mu = 2301.00832666667*xc[0]-0.203873368578 ;
        }

        else if (xc[0] <= 0.0000907)
        {
        mu = 3712.8117575*xc[0]-0.33135921838225;
        }

        else if (xc[0] <= 0.000091)
        {
        mu = 5696.13838*xc[0]-0.511246943043;
        }

        else if (xc[0] <= 0.0000915)
        {
        mu = 3638.638426*xc[0]-0.324014447229;
        }

        else if (xc[0] <= 0.000093)
        {
        mu = 0.126604423432-1286.15797466667*xc[0];
        }

        else if (xc[0] <= 0.000094)
        {
        mu = 0.05799630434-548.436264*xc[0];
```

```
                }

                else if (xc[0] <= 0.000101)
                {
                mu = 0.0100030141957143-37.8693475714286*xc[0];
                }

                else if (xc[0] <= 0.000102)
                {
                mu = 0.140559618586-1330.508995*xc[0];
                }

                else if (xc[0] <= 0.000103)
                {
                mu = 0.198957073318-1903.033061*xc[0];
                }

                else if (xc[0] <= 0.000105)
                {
                mu = 0.0719290609475-669.7513875*xc[0];
                }

                else if (xc[0] <= 0.000109)
                {
                mu = 45.1290915*xc[0]-0.0031333893475;
                }

                else if (xc[0] <= 0.000119)
                {
                mu = 0.0069279957175-47.1771935*xc[0];
                }

                else if (xc[0] <= 0.000122)
                {
                mu = 56.6566206666667*xc[0]-0.00542822816833333;
                }

                else if (xc[0] <= 0.000125)
                {
                mu = 374.614925666667*xc[0]-0.0442191413783333;
                }

                else if (xc[0] <= 0.0001309505)
                {
                mu = 629.99911553651*xc[0]-0.0761421651120637;
                }

                        else
                        {
                        mu = 4.3e-3;
                        }

return mu;

        }
```

```
/********************************************** ********************
UDF for 30 planes placed at varying lengths with
linear correlation for the viscosity
********************************************** ********************/

#include "udf.h"
DEFINE_PROPERTY(cell_viscosity, cell, thread)
{
        real xc[ND_ND];
        real mu;

                        C_CENTROID(xc, cell, thread);

                if (xc[0]< 0.0000037)
                {
                mu = 0.00132345128553305-3.73532933325807*xc[0];
                }

                else if (xc[0] <= 0.0000175)
                {
                mu = 1.561138623189*xc[0]+0.001303854354;
        }

                else if (xc[0] <= 0.000025)
                {
                mu = 0.0013815352247-2.8777682667*xc[0];
        }

                else if (xc[0]< 0.000035)
                {
                mu = 0.0013066371+0.1181565*xc[0];
                }

                else if (xc[0] <= 0.00004)
                {
                mu = 3.8410526*xc[0]+0.001176335742;
                }

                else if (xc[0] <= 0.0000465)
                {
                mu = 2.31464646153846*xc[0]+0.00123739198753846;
                }

                else if (xc[0] <= 0.00005)
                {
                mu = 0.001654922577-6.664506*xc[0];
                }

                else if (xc[0] <= 0.00006)
                {
                mu = 142.6701965*xc[0]-0.005811812548;
                }

                else if (xc[0] <= 0.000067)
                {
                mu =  116.257022285714*xc[0]-0.00422702209514;
                }
```

```
else if (xc[0] <= 0.000083)
{
mu = 0.01283720311675-138.43290625*xc[0];
}

else if (xc[0] <= 0.000087)
{
mu = 40.288708*xc[0]-0.001996690866;
}

else if (xc[0] <= 0.00009)
{
mu = 569.651364*xc[0]-0.048051241938;
}

else if (xc[0] <= 0.000091)
{
mu = 3884.268715*xc[0]-0.346366803528;
}

else if (xc[0] <= 0.000092)
{
  mu = 1698.150307*xc[0]-0.1474300284;
}

else if (xc[0] <= 0.000094)
{
mu = 0.117198998564-1178.25216*xc[0];
}

else if (xc[0] <= 0.000097)
{
mu = 0.004592034896+19.694262*xc[0];
}

else if (xc[0] <= 0.000101)
{
mu = 0.01436345762075-81.04205475*xc[0];
}

else if (xc[0] <= 0.000102)
{
mu = 0.140559618586-1330.508995*xc[0];
}

else if (xc[0] <= 0.000103)
{
mu = 0.1989570733-1903.033061*xc[0];
}

else if (xc[0] <= 0.000105)
{
mu = 0.0719290609475-669.7513875*xc[0];
}

else if (xc[0] <= 0.000109)
{
```

```
                mu = 45.1290915*xc[0]-0.0031333893475;
                }

                else if (xc[0] <= 0.000111)
                {
                mu = 0.0067398474385-45.4510625*xc[0];
                }

                else if (xc[0] <= 0.000114)
                {
                mu = 0.010871187426-82.6703416666667*xc[0];
                }

                else if (xc[0] <= 0.000119)
                {
                mu = 0.004475948774-26.571757*xc[0];
                }

                else if (xc[0] <= 0.0001205)
                {
                mu = 14.3438647*xc[0]-0.0003930102;
                }

                else if (xc[0] <= 0.000122)
                {
                mu = 98.9693766666667*xc[0]-0.0105903844003333;
                }

                else if (xc[0] <= 0.0001235)
                {
                mu = 266.686791333333*xc[0]-0.03105190899;
                }

                else if (xc[0] <= 0.000125)
                {
                mu = 482.54306*xc[0]-0.05771015817;
                }

                else if (xc[0] <= 0.00013)
                {
                mu = 192.8669156*xc[0]-0.02150064012;
                }

                else if (xc[0] <= 0.0001309505)
                {
                mu = 2929.48464913204*xc[0]-0.377260945479165;
                }

                else
                {
                mu = 3.45e-3;
                }

return mu;

        }
```

```
/************************************************************************
UDF for 30 planes placed at varying lengths with linear
correlation for the viscosity and hematocrit of 40
************************************************************************/

#include "udf.h"
DEFINE_PROPERTY(cell_viscosity, cell, thread)
{
        real xc[ND_ND];
        real mu;

                        C_CENTROID(xc, cell, thread);

                if (xc[0]< 0.0000037)
                {
                mu = 0.001292392978-3.69923837837838*xc[0];
                }

                else if (xc[0] <= 0.0000175)
                {
                mu = 1.49883289855072*xc[0]+0.00127316011427536;
                }

                else if (xc[0] <= 0.000025)
                {
                mu = 0.001347518022-2.7501904*xc[0];
                }

                else if (xc[0]< 0.000035)
                {
                mu = 0.025775*xc[0]+0.001278118887;
                }

                else if (xc[0] <= 0.00004)
                {
                mu = 2.1490182*xc[0]+0.001203805375;
                }

                else if (xc[0] <= 0.0000465)
                {
                mu = 3.39523569230769*xc[0]+0.00115395667530769;
                }

                else if (xc[0] <= 0.00005)
                {
                mu = 0.00159144020628571-6.01301228571429*xc[0];
                }

                else if (xc[0] <= 0.00006)
                {
                mu = 126.8885406*xc[0]-0.005053637438;
                }

                else if (xc[0] <= 0.000067)
                {
```

```
mu =  103.340479571429*xc[0]-0.00364075377628571;
}

else if (xc[0] <= 0.000083)
{
mu = 0.0115291202175625-123.0755501875*xc[0];
}

else if (xc[0] <= 0.000087)
{
mu = 35.88272175*xc[0]-0.00166441635325;
}

else if (xc[0] <= 0.00009)
{
mu = 506.390474666667*xc[0]-0.042598590857;
}

else if (xc[0] <= 0.000091)
{
mu = 3452.690983*xc[0]-0.307765636607;
}

else if (xc[0] <= 0.000092)
{
 mu = 1509.467475*xc[0]-0.130932297379;
}

else if (xc[0] <= 0.000094)
{
mu = 0.104293594537-1047.335698*xc[0];
}

else if (xc[0] <= 0.000097)
{
mu = 0.004198472763+17.506023*xc[0];
}

else if (xc[0] <= 0.000101)
{
mu = 0.01288418831025-72.03743625*xc[0];
}

else if (xc[0] <= 0.000102)
{
mu = 0.125058698096-1182.676147*xc[0];
}

else if (xc[0] <= 0.000103)
{
mu = 0.176968198436-1691.592817*xc[0];
}

else if (xc[0] <= 0.000105)
{
mu = 0.0640569767255-595.3673635*xc[0];
}
```

```
                else if (xc[0] <= 0.000109)
                {
                mu = 40.1218935*xc[0]-0.0026693952595;
                }

                else if (xc[0] <= 0.000111)
                {
                mu = 0.0061082137475-40.4066295*xc[0];
                }

                else if (xc[0] <= 0.000114)
                {
                mu = 0.009783280206-73.5153363333333*xc[0];
                }

                else if (xc[0] <= 0.000119)
                {
                mu = 0.004115451196-23.797538*xc[0];
                }

                else if (xc[0] <= 0.0001205)
                {
                mu = 13.1170573333333*xc[0]-0.000277385648666667;
                }

                else if (xc[0] <= 0.000122)
                {
                mu = 88.218364*xc[0]-0.009327093102;
                }

                else if (xc[0] <= 0.0001235)
                {
                mu = 237.110828666667*xc[0]-0.0274919737913333;
                }

                else if (xc[0] <= 0.000125)
                {
                mu = 428.943428*xc[0]-0.051183299809;
                }

                else if (xc[0] <= 0.00013)
                {
                mu = 171.4389218*xc[0]-0.018995236534;
                }

                else if (xc[0] <= 0.0001309505)
                {
                mu = 2602.62279074658*xc[0]-0.335049139497056;
                }

                        else
                        {
                        mu = 3.5e-3;
                        }

return mu;

        }
```